DISSERTATION | DOCTORAL THESIS

Titel | Title

Structural and Dynamic Characterization of the Intrinsically Disordered Protein YAP by NMR

verfasst von | submitted by

Michael Feichtinger BSc BA MSc

angestrebter akademischer Grad | in partial fulfilment of the requirements for the degree of

Doktor der Naturwissenschaften (Dr.rer.nat.)

Wien | Vienna, 2025

Studienkennzahl lt. Studienblatt | Degree programme code as it appears on the student record sheet:	UA 796 605 419
Dissertationsgebiet lt. Studienblatt | Field of study as it appears on the student record sheet:	Chemie
Betreut von | Supervisor:	Univ.-Prof. Dr. Robert Konrat

STRUCTURAL AND DYNAMIC CHARACTERIZATION OF THE INTRINSICALLY DISORDERED PROTEIN YAP BY NMR

Michael Feichtinger

Supervisor: Univ.-Prof. Dr. Robert Konrat

Time frame: 2018-2025

Location: Vienna, Austria

Acknowledgments

I want to thank my supervisor, Robert Konrat, for his steady support, encouragement, and for providing the space to pursue my own ideas. Your guidance helped shape this project and my understanding of what a nice academic environment can be.

To my colleagues at the department - Andreas Beier, Clemens Kauffmann, Tomáš Sára, Gerald Platzer, Sven Brüschweiler, Mario Migotti, Theresa Höfürthner, Karin Ledolter, Thomas Schwarz, Mate Somlyay and many more - thank you for all your help, the coffee breaks, and the shared frustrations and successes. Working with you made the ups and downs of research a lot more enjoyable.

To my partner Franziska, thank you for being there through it all. Your patience, love, and belief in me kept me going more than you know.

And to my parents, thank you for your endless support, for always believing in me, and for everything you've done to make this long journey possible.

Publications

The main body of this cumulative dissertation has previously been published as two scientific articles in peer-reviewed academic journals. Both are featured as separate chapters in Part II of the dissertation in order of appearance:

1. **Feichtinger M.,** Sára T., Platzer G., Mateos B., Bokhovchuk F., Chène P., Konrat R. (2018). "^{1}H, ^{13}C, ^{15}N resonance assignment of human YAP 50–171 fragment." *Biomolecular NMR Assignments*, 12(2), 179–182.
2. **Feichtinger M.,** Beier A., Migotti M., Schmid M., Bokhovchuk F., Chène P., Konrat R. (2022). "Long-range structural preformation in yes-associated protein precedes encounter complex formation with TEAD." *iScience*, 25(11), 104099.

In addition, the author contributed as a co-author to another peer-reviewed publication that was completed during the dissertation period but is not included as part of this thesis:

3. Schörghuber J., Geist L., Platzer G., **Feichtinger M.**, Bisaccia M., Scheibelberger L., Weber F., Konrat R., Lichtenecker R.J**.** (2018). "Late metabolic precursors for selective aromatic residue labeling." *Journal of Biomolecular NMR*, 71, 129–140.

Abstract

Intrinsically disordered proteins (IDPs) perform essential biological functions despite lacking stable three-dimensional structures. This dissertation explores the structural and dynamic properties of the IDP Yes-associated protein (YAP), a key regulator in the Hippo signaling pathway. Focusing on the TEAD-binding domain of YAP (residues 50–171), the work employs NMR spectroscopy to investigate the apo state and its role in TEAD interaction.

The first study provides a comprehensive backbone and partial side-chain resonance assignments, revealing transient secondary structural elements within the unbound YAP fragment. The presence of a β-strand, α-helix, and Ω-loop indicates that the apo state is not fully disordered, but instead exhibits structural preformation. Building on this, the second study demonstrates that these elements are co-stabilized through long-range intramolecular interactions. Paramagnetic relaxation enhancement (PRE), selective side-chain NOEs, and diffusion-ordered spectroscopy (DOSY) show that YAP adopts compact substates that bring critical binding elements into proximity. These conformations support a mechanism based on conformational selection rather than induced fit and are more compact than the bound state. Furthermore, this compact substate also presents new opportunities for therapeutic targeting.

In summary, this work provides the first atomic-level characterization of YAP's apo state, highlighting the functional role of structural preformation in IDPs. It supports a continuum model of protein function in which dynamic disorder contributes directly to molecular recognition and regulatory control.

Zusammenfassung

Intrinsisch ungeordnete Proteine (IDPs) erfüllen wichtige biologische Funktionen, obwohl ihnen eine stabile 3D-Struktur fehlt. Diese Dissertation untersucht die strukturellen und dynamischen Eigenschaften des IDPs Yes-associated protein (YAP), eines zentralen Regulators des Hippo-Signalwegs. Im Fokus steht die TEAD-Bindedomäne von YAP (50–171), deren apo-Zustand und Rolle in der TEAD-Interaktion mithilfe der NMR-Spektroskopie analysiert werden.

Die erste Studie liefert umfassende NMR-Signalzuordnung des Rückgrats und ausgewählter Seitenketten und zeigt dabei, dass im ungebundenen Zustand transiente sekundäre Strukturelemente vorhanden sind. Das Auftreten eines β-Strangs, einer α-Helix- und einer Ω-Schleife weisen darauf hin, dass der apo-Zustand nicht vollständig ungeordnet ist, sondern strukturelle Präformationen aufweist. Aufbauend darauf zeigt die zweite Studie, dass diese Elemente durch intramolekulare Wechselwirkungen stabilisiert werden. Paramagnetische Relaxationsverstärkung (PRE), selektive Seitenketten-NOEs und Diffusionsexperimente (DOSY) belegen, dass YAP kompakte Subzustände einnimmt, in denen die für die Bindung relevanten Elemente in räumliche Nähe gebracht werden. Diese Konformationen sprechen für einen Bindemechanismus basierend auf konformationeller Selektion anstelle eines induzierten Fits und sind sogar kompakter als der gebundene Zustand. Darüber hinaus eröffnet dieser kompakte Subzustand neue Ansatzpunkte für therapeutische Interventionen.

Insgesamt liefert diese Arbeit die erste Charakterisierung des apo-Zustands von YAP auf atomarer Ebene und hebt die funktionale Bedeutung struktureller Präformation bei IDPs hervor. Sie stützt ein Kontinuumsmodell für die Funktion von Proteinen, in dem dynamische Unordnung wesentlich zur molekularen Erkennung und Regulation beiträgt.

Table of Contents

PART I

Introduction

1) Proteins: A Very Short History

Proteins are macromolecules that perform a wide range of functions necessary for biological systems. They catalyze biochemical reactions, provide structural support, mediate cellular signals, and facilitate molecule transport across membranes[1]. Proteins occupy a central role in the modern framework of molecular biology, as they facilitate the flow of genetic information within a cell. This concept is famously encapsulated in the central dogma, which was first articulated by Francis Crick in 1958. This model outlines the flow of genetic information from DNA to RNA to protein. In this model, DNA holds the instructions for protein synthesis, which are transcribed to mRNA and then translated into amino acid sequences, forming proteins[2]. This sequential flow of information underscored the importance of proteins as the final expression of genetic code, which embody the functional and structural phenotypes of cells and organisms.

The foundational understanding of proteins dates back to the 19th century, but it was not until the 20th century that significant advancements were made in delineating their structure and function. Emil Fischer's introduction of the "lock and key" model for enzyme specificity published in 1894 provided a conceptual framework for understanding enzymatic action at a molecular level[3]. It is noteworthy that this discovery occurred prior to the initial publication of three-dimensional protein structures by decades. The full complexity of proteins was first appreciated in 1952 when Fred Sanger determined the amino acid sequence of insulin[4]. This landmark discovery demonstrated that proteins are sequences of amino acids linked by peptide bonds, underscoring the linear, primary structure of proteins and setting the stage for understanding their three-dimensional structures.

The methodological advancement that revolutionized our understanding of protein structure was X-ray crystallography, which provided a method to visualize the arrangement of atoms within a protein crystal. X-ray crystallography emerged as a

technique in structural biology following its initial successful application to sperm whale myoglobin[5] by Sir John Cowdery Kendrew in the late 1950s. This led to a Nobel Prize being awarded to Kendrew and Max Perutz in 1962. Kendrew's determination of the structure of myoglobin provided the first clear picture of a protein's complex three-dimensional structure, offering insights into the functions of proteins based on their shapes that were previously unavailable[6]. These and subsequent examples, such as the renowned hemoglobin structure[7], demonstrated the capacity of X-ray crystallography to elucidate the intricate three-dimensional structures and functions of proteins at the atomic level. By the end of the 20th century, thousands of protein structures had been resolved, each contributing to a deeper understanding of protein structure and function. Nevertheless, the findings collectively reinforced the prevailing view among researchers that all proteins must possess a well-defined structure in order to fulfill their functional roles. This dissertation will challenge this still widely held assumption.

2) Structure, Function and Dynamics

The already mentioned "lock and key" model for protein interaction, initially proposed by Fischer, was the first to demonstrate a connection between protein structure and function. According to this model, enzymes and their substrates interact with precision and specificity, akin to a key fitting into a lock[3]. This model underscores the belief that it needs preformed, rigid interaction sites on enzymes that perfectly match their substrates without necessitating structural changes upon binding. Daniel Koshland's induced fit model, introduced in 1958, extends the lock and key concept by proposing that the binding site of a protein undergoes a conformational adjustment upon binding. This adjustment enhances the binding affinity and catalytic efficiency by molding the structure around the binding partner, accommodating it more effectively[8]. In 1999, the conformational selection model was presented as an alternative. The conformational selection model diverges from the induced fit model in that it suggests that proteins exist in multiple

conformations even before the interaction event. Upon binding, the equilibrium shifts to stabilize the conformation that best fits the binding partner[9,10]. This model supports the idea of dynamic proteins whose functional states are determined by their interaction with other molecules, thereby highlighting the intrinsic flexibility of proteins. While these models provide valuable frameworks for understanding protein interactions, recent studies suggest that many proteins exhibit behavior that blends elements of these models. Such as that a protein may primarily use conformational selection to interact with a binding partner but subsequently undergoes further adjustments through an induced fit mechanism[11].

The discussed models of protein interaction illustrate how dynamic adaptations in protein structure are fundamental to their function. These models underscore that protein activity is not just about the presence of specific structures but also about the adaptability and responsiveness of these structures to physiological conditions. Intrinsically disordered proteins (IDPs), which are the main topic of this thesis, represent an extreme example of the importance of dynamic adaptations in the (un)structuring of proteins.

3) Intrinsically Disordered Proteins

Intrinsically disordered proteins (IDPs) represent a fascinating class of proteins that were first recognized around the turn of the new millennium to fulfill a broad range of biological functions without possessing a single fixed structure[12,13]. Since then, there has been a rapid growth in the field of studying IDPs, involving an increasing number of publications[14,15]. Due to their disordered nature, they challenge the traditional structure-function paradigm[16], which posits that a protein's function is dependent on its specific three-dimensional structure. This section will commence with a general characterization of IDPs, followed by an outline of their functional roles due to their dynamic nature. Finally, it will conclude with a discussion of some of the challenges in the study of IDPs.

Characteristics of IDPs

The defining property of IDPs is their lack of a stable secondary and tertiary structure under physiological conditions. Instead, IDPs exist as dynamic conformational ensembles with varying degrees of order and disorder[17]. This characteristic of IDPs is connected to a set of additional biophysical and chemical properties that are typically used to describe them.

On the level of amino acid sequences, IDPs are distinguished by their high proportion of disorder-promoting amino acids, including proline, glycine, and charged residues. These contribute to the lack of stable structures observed in IDPs. Furthermore, this amino acid composition facilitates a high degree of flexibility, allowing IDPs to exist in multiple conformations and respond dynamically to environmental changes[16,18]. In contrast, structured proteins typically exhibit a higher proportion of hydrophobic and aromatic amino acids, which facilitate the formation of a stable core through hydrophobic interactions and aromatic stacking[19]. A recent study on the sequence determinants of compaction of IDPs[20] has demonstrated that net charge and proline content are also the most significant predictors of IDP compaction, whereas hydrophobic interactions play a minimal role in most IDPs. The fact that compaction is not primarily driven by the formation of a hydrophobic core, but rather by transient collapsed structures and high conformational plasticity, results in the hydrodynamic radii of IDPs being on average larger than in folded proteins with comparable size[21].

Moreover, IDPs exhibit rapid backbone dynamics on a wide range of timescales, from picoseconds to milliseconds. This characteristic is not typically observed in structured proteins, which generally display more constrained and slower dynamics due to their stable tertiary structures. The rapid and diverse dynamic behaviors of IDPs additionally enables them to explore a larger conformational space[22].

Functional Roles of IDPs

The described flexibility allows IDPs to perform a wide range of biological functions, often playing crucial roles in protein interaction networks[23]. Within these networks, IDPs often serve as central hubs due to their structural flexibility, which enables them to function as targets for different binding partners. They are capable of binding to multiple partners with high specificity but low affinity, facilitating their involvement in diverse regulatory and signaling pathways[24]. Several IDPs also can bind to the same target as they are able to adopt their structures in accordance with their binding partners[13]. Furthermore, the ability of IDPs to interact in so-called fuzzy complexes is fundamental to many regulatory processes, allowing proteins to adapt their binding and function in response to cellular conditions. Such fuzziness adds adaptability, versatility and reversibility to protein interactions[25]. Moreover, protein disorder has been demonstrated to be significantly enriched in the vicinity of phosphorylation sites[26], indicating that IDPs or IDP regions within proteins serve as facilitators of post-translational modifications, thereby enabling additional regulatory mechanisms.

Due to their central roles in various regulatory mechanisms, alterations in the expression levels of IDPs are linked to several diseases, including cancer and neurodegenerative diseases[27]. One such IDP that is linked to cancer development is Yes-associated protein (YAP)[28–31], which is the main focus of this thesis. Regarding neurodegenerative disorders, well-known IDPs include tau, which plays a role in Alzheimer's disease[32], and α-synuclein in Parkinson's disease[33]. Therefore, targeting these IDPs presents a promising avenue for therapeutic interventions.

To account for the dynamic nature of IDPs, Gupta and Uversky proposed the concept of the protein structure-function continuum, which challenges the traditional binary classification of proteins as either structured or disordered. The concept of the structure-function continuum suggests that protein functionality exists along a continuous spectrum that encompasses fully structured to completely

disordered states. This continuum acknowledges that many proteins do not strictly adhere to a single, well-defined structure but may exhibit varying degrees of order and disorder depending on their functional requirements and cellular context[34].

Challenges in studying IDPs

Due to their high degree of functionality and conformational heterogeneity, the study of IDPs presents significant challenges. Traditional structural biology techniques, such as X-ray crystallography, often fail to provide meaningful insights into the structure of IDPs because these methods rely on crystalline order and static conformations[17]. It is not uncommon in X-ray crystallography to remove flexible parts of proteins to help crystallization, but, thereby, neglecting the importance of these regions[35]. Furthermore, the heterogeneity of IDPs and the presence of multiple conformational states within one sample make it difficult to characterize any specific state in isolation, as commonly used techniques, such as nuclear magnetic resonance (NMR) spectroscopy, provide average structural information. The same problem applies to very rapid and transient interactions that may be challenging to capture if below measurable timescales. Finally, the strength of IDPs is also a consequence of their responsiveness to the cellular environment. Consequently, they are particularly sensitive to experimental conditions, such as pH, temperature, and ionic strength.

Having explored the fundamental characteristics and the diverse roles of IDPs in cellular processes, the stage is set for a focused examination of YAP within the Hippo signaling pathway, which represents the main focus of this thesis and provides a prime example of how an IDP integrates into critical regulatory networks to control cellular outcomes.

4) YAP and the Hippo Pathway

The Hippo signaling pathway, first discovered about 20 years ago in *Drosophila melanogaster*, is highly conserved across various species, plays a crucial role in

regulating organ size, tissue homeostasis, and cellular processes such as proliferation, apoptosis, and stem cell renewal. This pathway's importance becomes especially apparent when considering its implications in human health and disease, particularly in cancer where its dysregulation can lead to unchecked cell growth and tumor development. As this thesis deals with the intrinsically disordered protein fragment of human YAP, only the mammalian/human hippo pathway will be discussed in this section.

At the heart of the Hippo pathway (see Fig. 1) are the MST1/2 kinases, which phosphorylate and activate the LATS1/2 kinases. These kinases, along with the scaffolding proteins SAV1 and MOB1A/B, form the central module of the pathway that regulates the activity of the transcription co-activators YAP and TAZ. Upon activation by MST1/2, LATS1/2 kinases phosphorylate YAP and TAZ, leading to their sequestration in the cytoplasm through binding to 14-3-3 proteins. This prevents their transcriptional activity in the nucleus, which serves as a critical checkpoint in preventing uncontrolled cell proliferation and promoting apoptosis when coupled with high cell density or other stress signals[36–38].

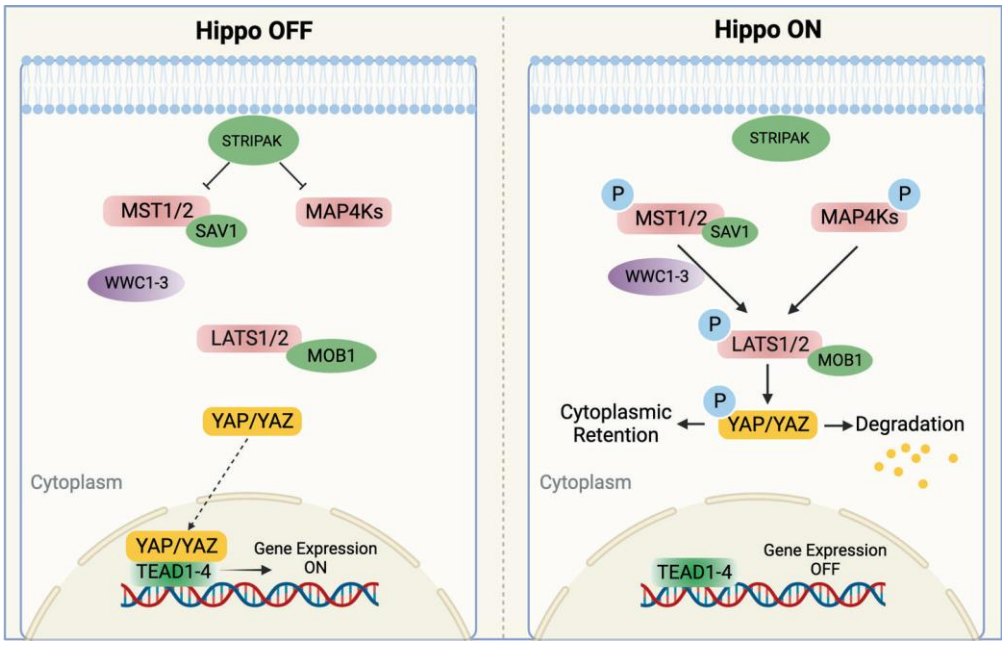

Fig. 1: An overview of the Hippo pathway and its central components [37].

Furthermore, the Hippo pathway does not operate in isolation but is engaged in extensive crosstalk with other signaling pathways, such as the Wnt/β-catenin, TGF-β, and JAK/STAT pathways. These interactions often modulate the activity of YAP and TAZ, integrating various signaling inputs to dictate cell fate decisions[39].

Dysregulation of the Hippo pathway has been implicated in numerous cancers, where mutations or altered expressions of pathway components lead to the hyperactivation of YAP and TAZ. Subsequently, these proteins are translocated to the nucleus, where they drive the expression of genes that promote cell proliferation and survival, thereby contributing to tumorigenesis and metastasis. Targeting the interaction between YAP/TAZ and their transcriptional partners, particularly TEA/ATTS domain transcription factors (TEAD), represents a promising strategy for therapeutic intervention, with the objective of curbing the oncogenic potential of YAP/TAZ hyperactivation[40,41]

Building on this understanding of the Hippo pathway, we will now focus on YAP and the specific fragment used in this dissertation, elucidating its specific role within this regulatory network. YAP acts as a terminal effector of the Hippo pathway by serving as a transcriptional co-activator through its interaction with TEAD transcription factors. This interaction is regulated by the phosphorylation of YAP on S127, which prevents its nuclear translocation by promoting binding to 14-3-3 proteins, thereby sequestering YAP in the cytoplasm[42]. The TEAD binding domain of YAP has been mapped to the protein region encompassing residues 50-100[43]. Several crystal structures of the YAP complex have been solved, providing detailed insights into the interaction between these two proteins[44–46]. These structures have revealed three key binding interfaces between YAP and TEAD: a β-strand (residues 52-58), an α-helix (residues 61-74), and an Ω-loop (residues 84-99). These secondary structure elements bind to distinct regions on the surface of TEAD. Mutational analyses have highlighted the critical importance of certain residues within these binding interfaces. Specifically, mutations in the α-helix and Ω-loop

significantly affect binding affinities, underscoring these regions as crucial for the YAP:TEAD interaction[46]. Previous studies demonstrated that the presence of both the α-helix and Ω-loop is necessary for high-affinity binding in the nanomolar range[47]. Furthermore, key residues of YAP and TEAD that constitute the YAP:TEAD binding site and their individual contribution to the binding have been described by site-directed mutagenesis studies[46]. They revealed that crucial residues for the interaction of the α-helix are L65, L68, and F69 which belong to the LxxLF motif that is known to bind to hydrophobic sites[44,48]. In a similar manner, the hydrophobic residues M86, L91 and F95 form a hydrophobic core within the Ω-loop region that interacts with TEAD. This core region is further stabilized by F96 through hydrophobic interactions. In addition, residues R89 and S94 interact via hydrogen bonds with TEAD. While the complex between the YAP-binding domain of TEAD and the TEAD-binding domain of YAP are already well characterized, there are hardly any data on the apo state YAP that is defined as intrinsically disordered protein[49].

For this dissertation that is supposed to investigate the structural dynamics of apo YAP and their potential effects on the YAP:TEAD complex formation, we have utilized the YAP fragment spanning residues 50-171. This particular fragment includes the crucial TEAD binding regions and extends beyond them to encompass additional regulatory elements that might influence YAP's interaction dynamics and functionality. Including the extended region up to residue 171 captures not only the essential binding interfaces but also additional phosphorylation sites and regions that may contribute to the protein's stability and regulatory mechanisms. The core methodological approach used to explore this intrinsically disordered protein fragment is NMR spectroscopy, which, as already mentioned above, is a powerful tool for studying the dynamic structures of IDPs.

5) NMR as a Tool for IDP Research

In contrast to traditional methods such as X-ray crystallography, which necessitate the formation of crystals and provide static structural snapshots, NMR spectroscopy enables researchers to investigate proteins in solution, capturing their dynamic behaviors and conformational ensembles. This capability is of particular importance for IDPs, whose functional mechanisms often depend on their flexibility and structural plasticity[18,50]. NMR spectroscopy operates on the principle that nuclei in a magnetic field absorb and re-emit electromagnetic radiation at characteristic frequencies. By applying a strong magnetic field and radiofrequency pulses to a sample, NMR can detect signals from specific types of nuclei, such as hydrogen (^{1}H), carbon (^{13}C), and nitrogen (^{15}N). These signals provide detailed information about the atomic environment, which can be used to infer information on the structure and dynamics of the protein[51,52].

During this thesis, several NMR techniques were employed that are suited for the study of IDPs. These included standard 2D experiments such as the ^{1}H-^{15}N HSQC, which is commonly used to provide information about the chemical environment of correlated ^{1}H and ^{15}N atoms. This is useful for identifying backbone amid groups in proteins. Additionally, 3D experiments, such as HNCA, HNCO, and NOESY, were employed. These experiments help in sequential assignment of resonances and in determining distances between nuclei through NOE correlations, which help to determine the spatial arrangement of atoms in proteins. Furthermore, paramagnetic relaxation enhancement (PRE) that involves the introduction of paramagnetic labels into the protein was heavily used[53]. The introduction of the paramagnetic label enhances relaxation rates and provides distance constraints between labeled sites and nearby nuclei. This technique is valuable for probing long-range interactions and transient conformations in IDPs, revealing how different regions of the protein come into proximity during its dynamic motions[54]. In addition, Diffusion-ordered spectroscopy (DOSY) were leveraged to measure the diffusion coefficients of

molecules in solution, which can be correlated with their size and shape[55]. For IDPs, DOSY provides insights into their overall dimensions and could provide additional information on compaction of IDPs. Finally, we made use of the combination of side-chain-specific labeling[56–58] with NOE detection which allowed for detailed mapping of side-chain interactions.

While NMR spectroscopy is a powerful tool, it is not without its own set of challenges, particularly when applied to IDPs. The use of high concentrations of isotopically labeled protein samples is necessary. Furthermore, the interpretation of NMR data for IDPs may exhibit broad and overlapping signals due to the small differences in the atomic environments of the specific residues. Both of these issues could prove challenging. For the used YAP fragment, we developed an expression protocol that yielded sufficient amounts of labeled protein. Due to the structural preformations in apo YAP that are described in this dissertation, the amount of signal overlap was also manageable.

6) Summary of the Publications

The first publication, "^{1}H, ^{13}C, ^{15}N resonance assignment of human YAP 50–171 fragment", focuses on the NMR resonance assignments for the YAP fragment spanning residues 50-171. This fragment encompasses the TEAD-binding domain, crucial for YAP's role in the Hippo pathway. The study provided detailed backbone and partial side-chain assignments, establishing a foundational dataset for further structural and dynamic studies of YAP in both its bound and unbound states. The chemical shift data revealed preformed secondary structure elements in the apo state, particularly the α-helix and β-strand regions, suggesting a degree of structural preformation that might facilitate binding to TEAD. This study underscored the intrinsically disordered nature of YAP while revealing specific structured regions critical for its function.

The second publication, "Long-range structural preformation in yes-associated protein precedes encounter complex formation with TEAD", expands on the previous work by combining various NMR techniques, site-directed mutagenesis, and affinity measurements to characterize the intrinsically disordered state of YAP. The findings demonstrated that the apo state of YAP adopts several compact conformations, which are crucial for the formation of the YAP complex. The study provided evidence that secondary structure elements, such as the α-helix and Ω-loop, are preformed and co-stabilized even before binding to TEAD. This preformation likely facilitates the rapid formation of the encounter complex through conformational selection. These insights are pivotal for understanding how YAP's intrinsic disorder and partial structuring contribute to its role in the Hippo pathway and its potential as a therapeutic target in cancer

Together, these publications advance our understanding of the functional mechanics of YAP within the Hippo pathway. By detailing the structural preformations in the apo state and binding interactions with TEAD, the studies highlight the importance of YAP's intrinsic disorder in enabling its diverse interactions and regulatory roles. In addition, the publications underscore the broader importance of studying IDPs in diverse biological contexts and serve as further examples that the concept of a structure-function continuum[34] is better suited to understanding protein function, which exists along a continuous spectrum from order to disorder.

7) References

1. Alberts, B. *et al. Molecular Biology of the Cell*. (W. W. Norton & Company, New York, 2022).
2. Crick, F. H. On protein synthesis. *Symp. Soc. Exp. Biol.* **12**, 138–163 (1958).
3. Fischer, E. Einfluss der Configuration auf die Wirkung der Enzyme. *Berichte Dtsch. Chem. Ges.* **27**, 2985–2993 (1894).
4. Sanger, F. The arrangement of amino acids in proteins. *Adv. Protein Chem.* **7**, 1–67 (1952).
5. Kendrew, J. C. *et al.* A three-dimensional model of the myoglobin molecule obtained by x-ray analysis. *Nature* **181**, 662–666 (1958).
6. Kendrew, J. C. The three-dimensional structure of a protein molecule. *Sci. Am.* **205**, 96–110 (1961).
7. Perutz, M. F., Kendrew, J. C. & Watson, H. C. Structure and function of haemoglobin. *J. Mol. Biol.* **13**, 669–678 (1965).
8. Koshland, D. E. Application of a Theory of Enzyme Specificity to Protein Synthesis. *Proc. Natl. Acad. Sci. U. S. A.* **44**, 98–104 (1958).
9. Ma, B., Kumar, S., Tsai, C.-J. & Nussinov, R. Folding funnels and binding mechanisms. *Protein Eng. Des. Sel.* **12**, 713–720 (1999).
10. Tsai, C., Kumar, S., Ma, B. & Nussinov, R. Folding funnels, binding funnels, and protein function. *Protein Sci.* **8**, 1181–1190 (1999).

11. Hammes, G. G., Chang, Y.-C. & Oas, T. G. Conformational selection or induced fit: A flux description of reaction mechanism. *Proc. Natl. Acad. Sci.* **106**, 13737–13741 (2009).
12. Tompa, P. Unstructural biology coming of age. *Curr. Opin. Struct. Biol.* **21**, 419–425 (2011).
13. Oldfield, C. J. & Dunker, A. K. Intrinsically Disordered Proteins and Intrinsically Disordered Protein Regions. *Annu. Rev. Biochem.* **83**, 553–584 (2014).
14. Uversky, V. N. Introduction to Intrinsically Disordered Proteins (IDPs). *Chem. Rev.* **114**, 6557–6560 (2014).
15. Uversky, V. N. & Kulkarni, P. Intrinsically disordered proteins: Chronology of a discovery. *Biophys. Chem.* **279**, 106694 (2021).
16. Wright, P. E. & Dyson, H. J. Intrinsically unstructured proteins: re-assessing the protein structure-function paradigm. *J. Mol. Biol.* **293**, 321–331 (1999).
17. Konrat, R. IDPs: Less Disordered and More Ordered than Expected. *Biophys. J.* **109**, 1309–1311 (2015).
18. Uversky, V. N. Natively unfolded proteins: A point where biology waits for physics. *Protein Sci.* **11**, 739–756 (2002).
19. Dunker, A. K. *et al.* Intrinsically disordered protein. *J. Mol. Graph. Model.* **19**, 26–59 (2001).
20. Marsh, J. A. & Forman-Kay, J. D. Sequence Determinants of Compaction in Intrinsically Disordered Proteins. *Biophys. J.* **98**, 2383–2390 (2010).

21. Uversky, V. N. Intrinsically Disordered Proteins and Their Environment: Effects of Strong Denaturants, Temperature, pH, Counter Ions, Membranes, Binding Partners, Osmolytes, and Macromolecular Crowding. *Protein J.* **28**, 305–325 (2009).

22. Eliezer, D. Biophysical characterization of intrinsically disordered proteins. *Curr. Opin. Struct. Biol.* **19**, 23–30 (2009).

23. Dunker, A. K., Cortese, M. S., Romero, P., Iakoucheva, L. M. & Uversky, V. N. Flexible nets The roles of intrinsic disorder in protein interaction networks. *FEBS J.* **272**, 5129–5148 (2005).

24. Tompa, P. & Fersht, A. *Structure and Function of Intrinsically Disordered Proteins*. (Chapman and Hall/CRC, 2009). doi:10.1201/9781420078930.

25. Tompa, P. & Fuxreiter, M. Fuzzy complexes: polymorphism and structural disorder in protein–protein interactions. *Trends Biochem. Sci.* **33**, 2–8 (2008).

26. Iakoucheva, L. M. The importance of intrinsic disorder for protein phosphorylation. *Nucleic Acids Res.* **32**, 1037–1049 (2004).

27. Babu, M. M., Van Der Lee, R., De Groot, N. S. & Gsponer, J. Intrinsically disordered proteins: regulation and disease. *Curr. Opin. Struct. Biol.* **21**, 432–440 (2011).

28. Ma, Y., Yang, Y., Wang, F., Wei, Q. & Qin, H. Hippo-YAP signaling pathway: A new paradigm for cancer therapy. *Int. J. Cancer* **137**, 2275–2286 (2015).

29. Pobbati, A. V. & Hong, W. Emerging roles of TEAD transcription factors and its coactivators in cancers. *Cancer Biol. Ther.* **14**, 390–398 (2013).

30. Pobbati, A. V. *et al.* Targeting the Central Pocket in Human Transcription Factor TEAD as a Potential Cancer Therapeutic Strategy. *Structure* **23**, 2076–2086 (2015).
31. Liu, A. M., Wong, K. F., Jiang, X., Qiao, Y. & Luk, J. M. Regulators of mammalian Hippo pathway in cancer. *Biochim. Biophys. Acta - Rev. Cancer* **1826**, 357–364 (2012).
32. Skrabana, R., Skrabanova, M., Csokova, N., Sevcik, J. & Novak, M. Intrinsically disordered tau protein in Alzheimer's tangles: a coincidence or a rule? *Bratisl. Lek. Listy* **107**, 354–358 (2006).
33. Brash-Arias, D. *et al.* The Role of Astrocytes and Alpha-Synuclein in Parkinson's Disease: A Review. *NeuroSci* **5**, 71–86 (2024).
34. Gupta, M. N. & Uversky, V. N. Protein structure–function continuum model: Emerging nexuses between specificity, evolution, and structure. *Protein Sci.* **33**, e4968 (2024).
35. Dale, G. E., Oefner, C. & D'Arcy, A. The protein as a variable in protein crystallization. *J. Struct. Biol.* **142**, 88–97 (2003).
36. Yu, F.-X., Zhao, B. & Guan, K.-L. Hippo Pathway in Organ Size Control, Tissue Homeostasis, and Cancer. *Cell* **163**, 811–828 (2015).
37. Fu, M. *et al.* The Hippo signalling pathway and its implications in human health and diseases. *Signal Transduct. Target. Ther.* **7**, 376 (2022).
38. Ma, S., Meng, Z., Chen, R. & Guan, K.-L. The Hippo Pathway: Biology and Pathophysiology. *Annu. Rev. Biochem.* **88**, 577–604 (2019).

39. Zhao, B., Lei, Q.-Y. & Guan, K.-L. The Hippo–YAP pathway: new connections between regulation of organ size and cancer. *Curr. Opin. Cell Biol.* **20**, 638–646 (2008).

40. Piccolo, S., Dupont, S. & Cordenonsi, M. The Biology of YAP/TAZ: Hippo Signaling and Beyond. *Physiol. Rev.* **94**, 1287–1312 (2014).

41. Chapeau, E. A. *et al.* Direct and selective pharmacological disruption of the YAP–TEAD interface by IAG933 inhibits Hippo-dependent and RAS–MAPK-altered cancers. *Nat. Cancer* (2024) doi:10.1038/s43018-024-00754-9.

42. Zhao, B. *et al.* Inactivation of YAP oncoprotein by the Hippo pathway is involved in cell contact inhibition and tissue growth control. *Genes Dev.* **21**, 2747–2761 (2007).

43. Vassilev, A., Kaneko, K. J., Shu, H., Zhao, Y. & Depamphilis, M. L. YAP65 , a Src / Yes-associated protein localized in the cytoplasm TEAD / TEF transcription factors utilize the activation domain of YAP65 , a Src / Yes-associated protein localized in the cytoplasm. *Genes Dev.* **15**, 1229–1241 (2001).

44. Li, Z. *et al.* Structural insights into the YAP and TEAD complex service Structural insights into the YAP and TEAD complex. *Genes Dev.* 235–240 (2010) doi:10.1101/gad.1865810.

45. Chen, L., Chan, S. W., Zhang, X., Walsh, M. & Lim, C. J. Structural basis of YAP recognition by TEAD4 in the Hippo pathway Structural basis of YAP recognition by TEAD4 in the Hippo pathway. *Genes Dev.* 290–300 (2010) doi:10.1101/gad.1865310.

46. Mesrouze, Y. *et al.* Dissection of the interaction between the intrinsically disordered YAP protein and the transcription factor TEAD. *eLife* **6**, 1–16 (2017).

47. Hau, J. C. *et al.* The TEAD4-YAP/TAZ Protein-Protein Interaction: Expected Similarities and Unexpected Differences. *ChemBioChem* **14**, 1218–1225 (2013).

48. Santucci, M. *et al.* The Hippo Pathway and YAP/TAZ-TEAD Protein-Protein Interaction as Targets for Regenerative Medicine and Cancer Treatment. *J. Med. Chem.* **58**, 4857–4873 (2015).

49. Tian, W., Yu, J., Tomchick, D. R., Pan, D. & Luo, X. Structural and functional analysis of the YAP-binding domain of human TEAD2. *Proc. Natl. Acad. Sci. U. S. A.* **107**, 7293–7298 (2010).

50. Dyson, H. J. & Wright, P. E. Intrinsically unstructured proteins and their functions. *Nat. Rev. Mol. Cell Biol.* **6**, 197–208 (2005).

51. Wüthrich, K. *NMR of Proteins and Nucleic Acids*. (Wiley, New York, 1986).

52. *Protein NMR Spectroscopy: Principles and Practice*. (Academic Press, Amsterdam ; Boston, 2007).

53. Kosen, P. A. Spin labeling of proteins. *Methods Enzymol.* **177**, 86–121 (1989).

54. Jensen, M. R., Ruigrok, R. W. & Blackledge, M. Describing intrinsically disordered proteins at atomic resolution by NMR. *Curr. Opin. Struct. Biol.* **23**, 426–435 (2013).

55. Morris, G. A. Diffusion-Ordered Spectroscopy. in *Encyclopedia of Magnetic Resonance* (ed. Harris, R. K.) emrstm0119.pub2 (John Wiley & Sons, Ltd, Chichester, UK, 2009). doi:10.1002/9780470034590.emrstm0119.pub2.

56. Lichtenecker, R. J., Weinhäupl, K., Schmid, W. & Konrat, R. α-Ketoacids as precursors for phenylalanine and tyrosine labelling in cell-based protein overexpression. *J. Biomol. NMR* **57**, 327–331 (2013).

57. Lichtenecker, R. J., Coudevylle, N., Konrat, R. & Schmid, W. Selective Isotope Labelling of Leucine Residues by Using α-Ketoacid Precursor Compounds. *ChemBioChem* **14**, 818–821 (2013).

58. Klopp, J. *et al.* Cost-effective large-scale expression of proteins for NMR studies. *J. Biomol. NMR* **1**, 0 (2018).

PART II

Collection of Published Articles

The core of this cumulative thesis consists of two self-contained scientific articles that investigate the structural and dynamic properties of the intrinsically disordered protein YAP and their influence on its interaction with the transcription factor TEAD, primarily using NMR spectroscopy. Both articles have been published in peer-reviewed scientific journals under a Creative Commons Attribution 4.0 International (CC BY 4.0) license and can therefore be reproduced in this dissertation in their original layout and formatting. Where applicable, supporting figures and tables are included in their published form. At the beginning of each chapter, the corresponding digital object identifier (DOI) is provided alongside a brief statement outlining the author's individual contribution.

8) ^{1}H, ^{13}C, ^{15}N RESONANCE ASSIGNMENT OF HUMAN YAP 50–171 FRAGMENT

Feichtinger, M., Sára, T., Platzer, G., Mateos, B., Bokhovchuk, F., Chéne, P., Konrat, R. ^{1}H, ^{13}C, ^{15}N resonance assignment of human YAP 50–171 fragment. *Biomol NMR Assign* **12**, 179–182 (2018)

DOI: 10.1007/s12104-018-9805-8

Personal Contribution: Protein production, execution of experiments, data analysis and validation, writing of the article

Biomolecular NMR Assignments (2018) 12:179–182
https://doi.org/10.1007/s12104-018-9805-8

ARTICLE

^{1}H, ^{13}C, ^{15}N resonance assignment of human YAP 50–171 fragment

Michael Feichtinger[1] · Tomáš Sára[1] · Gerald Platzer[1] · Borja Mateos[1] · Fedir Bokhovchuk[2] · Patrick Chène[2] · Robert Konrat[1]

Received: 29 November 2017 / Accepted: 23 January 2018 / Published online: 25 January 2018

Abstract
Yes associated protein (YAP) is an intrinsically disordered protein that plays a major role in the Hippo pathway, regulating organ size, cell proliferation, apoptosis, and is associated with cancer development. Therefore, the binding between YAP and TEAD is an interesting target for cancer therapy. The TEAD binding domain of YAP was mapped to protein residues 50–171. To obtain further structural insights into this 12 kDa segment of YAP, we report a backbone and a partial sidechain assignment of recombinant YAP 50–171.

Keywords YAP · Intrinsically disordered protein · Hippo pathway · NMR · TEAD

Biological context

Yes associated protein (YAP) is an partly intrinsically disordered protein transcribed into four different isoforms ranging from 326 to 504 residues (Santucci et al. 2015). YAP is a major target and a terminal effector of the Hippo pathway, important for the regulation of organ size (Zhao et al. 2011) and is associated with cancer development (Liu et al. 2012; Pobbati and Hong 2013; Ma et al. 2015; Pobbati et al. 2015). One of the functions of YAP is to bind to the TEAD transcription factors as a transcriptional coactivator. Therefore, the YAP:TEAD interaction might be a promising therapeutic approach in cancers where the Hippo pathway is deregulated. The formation of the YAP:TEAD complex is indirectly regulated by YAP phosphorylation, which prohibits nuclear translocation of YAP and leads to downregulation of genes related to proliferation; therefore, leading to apoptosis (Zhao et al. 2007).

Previously, the binding between YAP and TEAD was studied and the protein region 50–171 was identified as the TEAD binding domain (Vassilev et al. 2001) Furthermore, three binding interfaces were identified between YAP and TEAD (Li et al. 2010). Namely, a β-strand (residues 52–58), an α-helix (residues 61–73), and an Ω-loop (residues 86–100). Furthermore, key residues in the binding site and their contribution to the binding have been described (Mesrouze et al. 2017).

In order to gain further insights into the binding process and structural features of the bound and unbound state, we present a chemical shift assignment of YAP 50–171.

Methods and experiments

Sample preparation

The sequence coding for YAP residues 50–171 was amplified by PCR and cloned into a pETM14 vector by sequence and ligation independent cloning (SLIC) (Scholz et al. 2013). The plasmid, containing the fusion protein with a His6-tag at the N-terminus and a 3C protease cleavage site, was transformed into *Escherichia coli* Tuner™(DE3). Four liters of LB medium were inoculated with the overnight culture and incubated at 37 °C until an OD_{600} of 0.8. Cells were centrifuged and all pellets were combined and resuspended in one liter of M9 minimal medium containing 1 g/L ^{15}N ammonium chloride (Sigma Aldrich) and 3 g/L ^{13}C glucose (Cambridge Isotope) as the sole source of nitrogen and carbon, respectively (Marley et al. 2001). After an additional hour at 37 °C, expression was induced with the addition of

✉ Robert Konrat
robert.konrat@univie.ac.at

[1] Max F. Perutz Laboratories, Department of Computational and Structural Biology, University of Vienna, Campus Vienna Biocenter 5, 1030 Vienna, Austria

[2] Disease Area Oncology, Novartis Institutes for Biomedical Research, 141 Klybeckstrasse, 4057 Basel, Switzerland

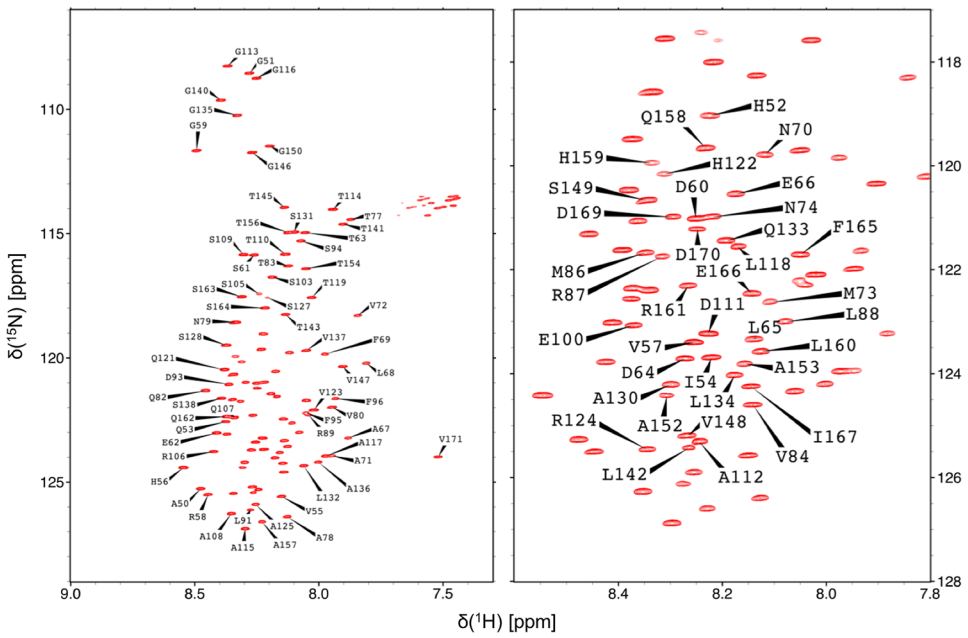

Fig. 1 Left ^{1}H–^{15}N TROSY HSQC spectrum of YAP 50–171 at pH 6 and 298 K. Right magnification of the central region of the spectrum

0.8 mM IPTG and cells were incubated for 18 h at 30 °C and consecutively harvested by centrifugation and stored at − 20 °C.

Frozen cell pellets were resuspended in lysis buffer (20 mM Tris, 150 mM NaCl, 30 mM Imidazole, pH 7.8), supplemented with 50 µL of Protease Inhibitor Cocktail (Thermo Scientific), and lysed by sonication on ice. Lysate was clarified by centrifugation and supernatant was loaded onto a HisTrap FF column and washed with 8 column volumes of wash buffer (20 mM Tris, 150 mM NaCl, 40 mM Imidazole, pH 7.8). After eluting with 15 ml of elution buffer (20 mM Tris, 150 mM NaCl, 300 mM Imidazole, 1 mM EDTA, pH 7.8), the eluate was concentrated to 2 ml and dialyzed overnight against an excess of NMR buffer (20 mM BisTris, 150 mM NaCl, 1 mM EDTA, pH 6.0). Consequently, His6-tag was removed by 3C protease cleavage overnight at 4 °C. NaCl was added to a final concentration of 1 M and the solution was heated to 90 °C for 10 min. After centrifugation, the supernatant was loaded onto a HiLoad 16/600 (GE Healthcare) size exclusion column equilibrated with NMR buffer. Purified protein, which was > 95% pure as assessed by SDS/PAGE, was concentrated to approximately 0.5 mM in NMR buffer containing 10% D_2O as determined by Pierce BCA Protein Assay (Thermo Scientific).

NMR spectroscopy

NMR experiments were performed at 298 K using a Bruker Avance III 800 MHz spectrometer. The backbone assignments were obtained using BEST-TROSY type versions of HNCANNH, HN(COCA)NNH, HNCACB, HN(CO)CACB, HNCO, and HN(CA)CO experiments (Solyom et al. 2013). Data was processed with NMRPipe (Delaglio et al. 1995) and spectra were assigned using CcpNmr (Vranken et al. 2005) and Sparky (Goddard and Kneller 2004).

Assignments and data deposition

Assignment of the backbone amides ^{1}H, ^{15}N of YAP 50–171 is shown in Fig. 1. Backbone amide resonances were assigned for all of 108 non-proline residues, except of K76, K90, K97, K102, H104, and H126. Therefore, 12% of the total ^{1}H resonances of the protein were assigned. In addition, 94% of Cα and Cβ resonances of the respective residues and 81% of C' resonances were assigned. The very narrow peak dispersion in the ^{1}H dimension of the ^{1}H–^{15}N HSQC spectrum shows that YAP 50–171 is intrinsically disordered. Nevertheless, the secondary structure propensity (SSP) score (Marsh et al. 2006) clearly indicates a propensity for a preformation of the α-helix and the N-terminal β-strand in the unbound state (Fig. 2a). The protein region of the Ω-loop shows no exceptional SSP scores. Furthermore, the protein seems to preferentially adopt extended structures (negative SSP scores).

The ^{1}H, ^{13}C and ^{15}N chemical shifts have been deposited in the BioMagResBank (http://www.bmrb.wisc.edu/) under the BMRB accession number 27290.

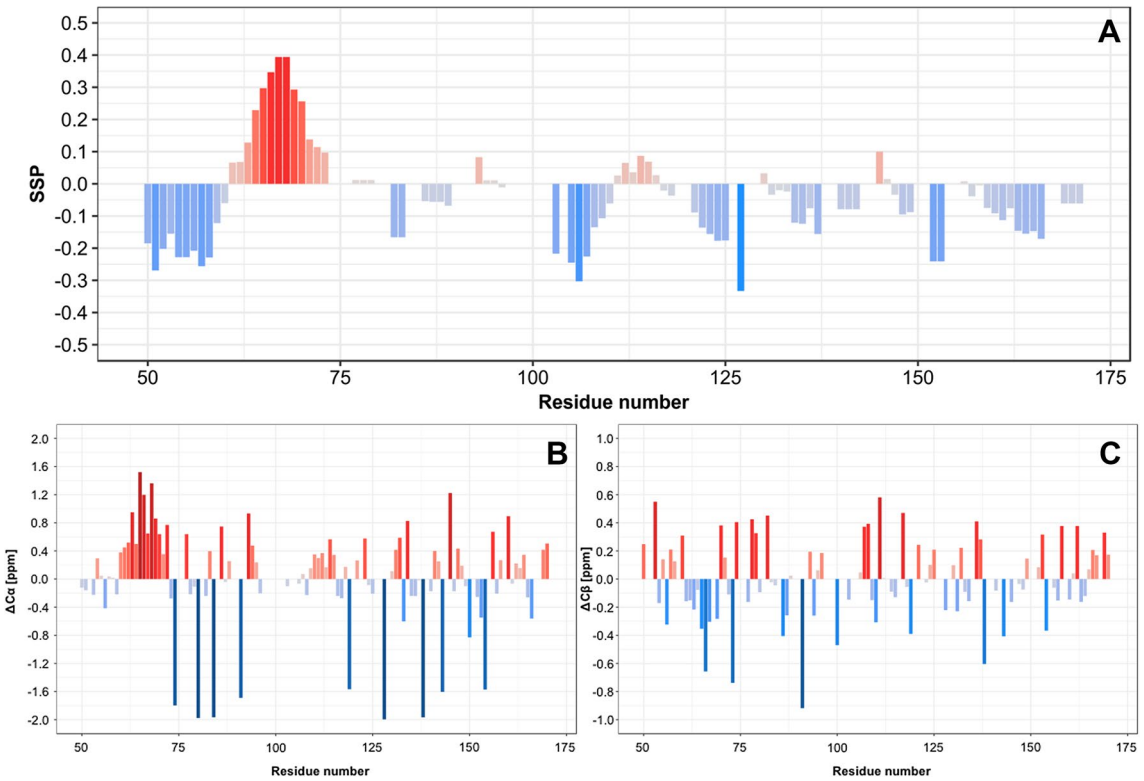

Fig. 2 **a** SSP score (Marsh et al. 2006) of YAP 50–171 at pH 6 and 298 K. Positive scores indicate a propensity for α-helical structures, whereas β-strands or extended structural elements possess a negative score. The calculation of the SSP score was performed with all available chemical shift data. **b** Cα chemical shift deviations from random coil values (Zhang et al. 2003). **c** Cβ chemical shift deviations from random coil values

Acknowledgements Open access funding provided by Austrian Science Fund (FWF). The authors thank Georg Kontaxis for pulse sequence programming and general NMR expertise. Funding for the work was provided by the special doctoral program "Integrative Structural Biology" of the Austrian Science Foundation (FWF) and the Christian Doppler Laboratory for High-Content Structural Biology and Biotechnology, Austria.

References

Delaglio F, Grzesiek S, Vuister GW et al (1995) NMRPipe: a multidimensional spectral processing system based on UNIX pipes. J Biomol NMR 6:277–293. https://doi.org/10.1007/BF00197809

Goddard TD, Kneller DG (2004) Sparky 3. University of California, San Francisco

Li Z, Zhao B, Wang P et al (2010) Structural insights into the YAP and TEAD complex service structural insights into the YAP and TEAD complex. Genes Dev 235–240. https://doi.org/10.1101/gad.1865810

Liu AM, Wong KF, Jiang X et al (2012) Regulators of mammalian Hippo pathway in cancer. Biochim Biophys Acta 1826:357–364. https://doi.org/10.1016/j.bbcan.2012.05.006

Ma Y, Yang Y, Wang F et al (2015) Hippo-YAP signaling pathway: a new paradigm for cancer therapy. Int J Cancer 137:2275–2286. https://doi.org/10.1002/ijc.29073

Marley J, Lu M, Bracken C (2001) A method for efficient isotopic labeling of recombinant proteins. J Biomol NMR 20:71–75. https://doi.org/10.1023/A:1011254402785

Marsh J, Singh VK, Jia Z, Forman-Kay JD (2006) Sensitivity of secondary structure propensities to sequence differences between alpha- and gamma-synuclein: implications for fibrillation. Protein Sci 15:2795–2804. https://doi.org/10.1110/ps.062465306

Mesrouze Y, Bokhovchuk F, Meyerhofer M et al (2017) Dissection of the interaction between the intrinsically disordered YAP protein and the transcription factor TEAD. Elife 6:1–16. https://doi.org/10.7554/eLife.25068.001

Pobbati AV, Hong W (2013) Emerging roles of TEAD transcription factors and its coactivators in cancers. Cancer Biol Ther 14:390–398. https://doi.org/10.4161/cbt.23788

Pobbati AV, Han X, Hung AW et al (2015) Targeting the central pocket in human transcription factor TEAD as a potential cancer therapeutic strategy. Structure 23:2076–2086. https://doi.org/10.1016/j.str.2015.09.009

Santucci M, Vignudelli T, Ferrari S et al (2015) The Hippo pathway and YAP/TAZ-TEAD protein-protein interaction as targets for regenerative medicine and cancer treatment. J Med Chem 58:4857–4873. https://doi.org/10.1021/jm501615v

Scholz J, Besir H, Strasser C, Suppmann S (2013) A new method to customize protein expression vectors for fast, efficient and background free parallel cloning. BMC Biotechnol 13:12. https://doi.org/10.1186/1472-6750-13-12

Solyom Z, Schwarten M, Geist L et al (2013) BEST-TROSY experiments for time-efficient sequential resonance assignment of large disordered proteins. J Biomol NMR 55:311–321. https://doi.org/10.1007/s10858-013-9715-0

Vassilev A, Kaneko KJ, Shu H et al (2001) YAP65, a Src/Yes-associated protein localized in the cytoplasm TEAD/TEF transcription factors utilize the activation domain of YAP65, a Src/Yes-associated protein localized in the cytoplasm. Genes Dev 15:1229–1241. https://doi.org/10.1101/gad.888601

Vranken WF, Boucher W, Stevens TJ et al (2005) The CCPN data model for NMR spectroscopy: development of a software pipeline. Proteins Struct Funct Genet 59:687–696. https://doi.org/10.1002/prot.20449

Zhang H, Neal S, Wishart DS (2003) RefDB: a database of uniformly referenced protein chemical shifts. J Biomol NMR 25:173–195

Zhao B, Zhao B, Wei X et al (2007) Inactivation of YAP oncoprotein by the Hippo pathway is involved in cell contact inhibition and tissue growth control. Genes Dev 21:2747–2761. https://doi.org/10.1101/gad.1602907.Hpo/Sav

Zhao B, Tumaneng K, Guan KL (2011) The Hippo pathway in organ size control, tissue regeneration and stem cell self-renewal. Nat Cell Biol 13:877–883. https://doi.org/10.1038/ncb2303

9) LONG-RANGE STRUCTURAL PREFORMATION IN YES-ASSOCIATED PROTEIN PRECEDES ENCOUNTER COMPLEX FORMATION WITH TEAD

Feichtinger, M., Beier, A., Migotti, M., Schmid, M., Bokhovchuk, F., Chéne, P., Konrat, R. Long-range structural preformation in yes-associated protein precedes encounter complex formation with TEAD. *iScience* **25**, 104099 (2022)

DOI: 10.1016/j.isci.2022.104099

Personal Contribution: Protein production, design and execution of experiments, data validation and analysis, writing of the article

iScience

CellPress
OPEN ACCESS

Article

Long-range structural preformation in yes-associated protein precedes encounter complex formation with TEAD

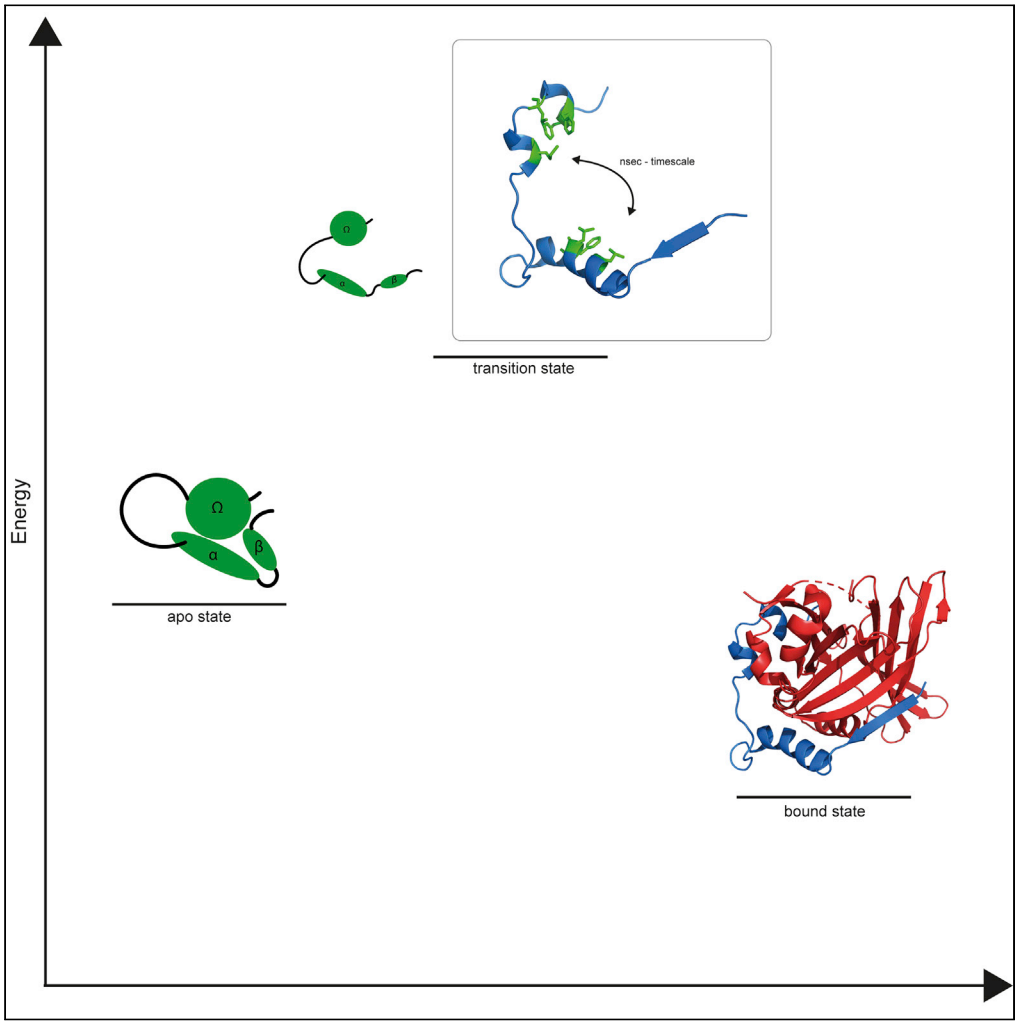

Michael Feichtinger, Andreas Beier, Mario Migotti, Matthias Schmid, Fedir Bokhovchuk, Patrick Chène, Robert Konrat

michael.feichtinger@univie.ac.at

Highlights

Secondary structure elements are preformed in apo YAP

Preformation of secondary structure elements is co-dependent

Apo YAP exhibits long-range structural compaction

YAP compaction has a kinetic contribution to the YAP:TEAD formation

Feichtinger et al., iScience 25, 104099
April 15, 2022
https://doi.org/10.1016/j.isci.2022.104099

iScience

CellPress
OPEN ACCESS

Article

Long-range structural preformation in yes-associated protein precedes encounter complex formation with TEAD

Michael Feichtinger,[1,4,*] Andreas Beier,[1] Mario Migotti,[1] Matthias Schmid,[1] Fedir Bokhovchuk,[2] Patrick Chène,[3] and Robert Konrat[1]

SUMMARY

Yes-associated protein (YAP) is a partly intrinsically disordered protein (IDP) that plays a major role as the downstream element of the Hippo pathway. Although the structures of the complex between TEA domain transcription factors (TEADs) and the TEAD-binding domain of YAP are already well characterized, its apo state and the binding mechanism with TEADs are still not clearly defined. Here we characterize via a combination of different NMR approaches with site-directed mutagenesis and affinity measurements the intrinsically disordered solution state of apo YAP. Our results provide evidence that the apo state of YAP adopts several compact conformations that may facilitate the formation of the YAP:TEAD complex. The interplay between local secondary structure element preformation and long-range co-stabilization of these structured elements precedes the encounter complex formation with TEAD and we, therefore, propose that TEAD binding proceeds largely via conformational selection of the preformed compact substates displaying at least nanosecond lifetimes.

INTRODUCTION

YAP (Yes-Associated Protein) is a partly intrinsically disordered protein (IDP) that serves as one of the terminal effectors of the Hippo pathway. This pathway plays a central role in regulating organ size, cell differentiation, and regeneration (Moya and Halder, 2019; Tremblay and Camargo, 2012; Wang et al., 2017; Zhao et al., 2011). One of the main functions of YAP is to bind the TEA/ATTS domain transcription factors (TEADs), as a transcriptional co-activator. Together, YAP and TEAD form a functional transcription complex that induces the expression of Hippo-responsive genes (Pobbati et al., 2015; Pobbati and Hong, 2013). The formation of the YAP:TEAD complex is regulated by YAP phosphorylation on S127, which prohibits the nuclear translocation of YAP via 14-3-3 binding and leads to the downregulation of genes related to proliferation, therefore, leading to apoptosis (Zhao et al., 2007). The phosphorylation of YAP is a result of the activation of the core kinase cassette of the Hippo pathway and occurs in the cytoplasm (Ma et al., 2019). Thus, phosphorylation at S127 leads to cytoplasmic retention via binding to 14-3-3 proteins (Zhao et al., 2007). The deregulation of the Hippo pathway is associated with cancer development (Liu et al., 2012; Ma et al., 2015; Pobbati et al., 2015; Pobbati and Hong, 2013) and, therefore, the inhibition of the YAP:TEAD interaction might be a promising therapeutic approach in cancers where the Hippo pathway is deregulated (Calses et al., 2019; Holden and Cunningham, 2018; Santucci et al., 2015; Ye and Eisinger-Mathason, 2016).

The TEAD binding domain of YAP was mapped to the protein region 50-100 (Vassilev et al., 2001), and several crystal structures of YAP:TEAD complexes have been solved in recent years (Chen et al., 2010; Li et al., 2010; Mesrouze et al., 2017). These structures revealed three binding interfaces between YAP and TEAD: a β-strand (residues 52-58), an α-helix (residues 61-74), and an Ω-loop (residues 84-99). These three secondary structure elements bind to distinct regions at the surface of TEAD. It was shown that the mutation of certain residues in the α-helix and Ω-loop strongly affects binding affinities which lead to the conclusion that these two sites form the crucial binding interfaces in the YAP:TEAD interaction (Mesrouze et al., 2017). In addition, previous studies demonstrated that the presence of the α-helix and Ω-loop are necessary for binding with nanomolar affinity (Hau et al., 2013). Furthermore, key residues of YAP and TEAD that constitute the YAP:TEAD binding site and their individual contribution to the binding have been described

[1]Department of Computational and Structural Biology, Max Perutz Labs, University of Vienna, Campus Vienna Biocenter 5, 1030 Vienna, Austria

[2]Ichnos Sciences SA, Route de la Corniche 5A, 1066 Epalinges, Switzerland

[3]Novartis Pharma AG, Postfach WSJ 386.4, 4002 Basel, Switzerland

[4]Lead contact

*Correspondence: michael.feichtinger@univie.ac.at

https://doi.org/10.1016/j.isci.2022.104099

by site-directed mutagenesis studies (Mesrouze et al., 2017). They revealed that crucial residues for the interaction of the α-helix are L65, L68, and F69 which belong to the LxxLF motif that is known to bind to hydrophobic sites (Li et al., 2010; Santucci et al., 2015). In a similar manner, the hydrophobic residues M86, L91, and F95 form a hydrophobic core within the Ω-loop region that interacts with TEAD. This core region is further stabilized by F96 through hydrophobic interactions. In addition, residues R89 and S94 interact via hydrogen bonds with TEAD. The mutations of these residues to Ala showed significant effects (ΔΔG from 1.9 to 4.4 kcal/mol) on the binding affinity between YAP and TEAD (Mesrouze et al., 2017).

While the complex between the YAP-binding domain of TEAD and the TEAD-binding domain of YAP is already well characterized, there are hardly any data on the apo state of the TEAD-binding domain of YAP that is defined as intrinsically disordered protein in the apo state (Feichtinger et al., 2018; Tian et al., 2010).

As already indicated, the YAP:TEAD interaction might be a promising therapeutic approach in cancers where the Hippo pathway is deregulated. However, there are some reports in the area of small molecules targeting the YAP:TEAD transcriptional activation complex with moderate levels of pathway inhibition (Crawford et al., 2018). Interestingly, it has been shown that Verteporfin, known to disrupt the YAP:TEAD interaction, is co-eluting with YAP and not with TEAD on a size exclusion column, and therefore, suggested to bind to YAP (Liu-chittenden et al., 2012). Even if further research has shown that porphyrin- and dipyrrin-related derivatives can directly target YAP (Gibault et al., 2017), the mechanism behind the inhibition effect of Verteporfin and these derivatives remains to be elucidated as there is no structural information on the apo state of YAP. In summary, all the studies carried out so far have mainly focused on the bound state of YAP to TEAD, mainly owing to the insufficiency of the applied methods for characterizing the intrinsically disordered YAP protein in the free form on an atomic level. The predominating opinion in the field is that the TEAD-binding domain of YAP is completely disordered and folds upon binding to TEAD.

In this article, we combine different NMR approaches with site-directed mutagenesis and affinity measurements to characterize the intrinsically disordered state of YAP. We present evidence that the apo state of YAP adopts several ordered conformations that may facilitate the formation of the YAP:TEAD complex.

RESULTS

Secondary structure elements are preformed in apo YAP

We obtained straightforward evidence that YAP^{50-171} (hereafter referred to as YAP^{wt}) possesses all three described secondary structure elements (β-strand, α-helix, and Ω-loop) in the apo state through the combination of chemical shift data, ^{15}N relaxation measurements, and site-specific precursor labeling paired with NOE experiments. The secondary structure propensity (SSP) scores (Marsh et al., 2006) derived from the chemical shift data of the ^{1}H, ^{13}C, and ^{15}N and -assignment of YAP (Feichtinger et al., 2018) clearly indicate a propensity for a preformation of an extended structure in the N-terminus of the protein corresponding to the β-strand region and the α-helix in the unbound state (Figure 1A). In particular, the helical region spanning from residue 61-73 in the YAP:TEAD complex shows a strong helical propensity up to an SSP of 0.4 representing the helical population. Residues located in the Ω-loop show no increased SSP scores as this method is not applicable to non-canonical secondary structure elements. This observation of the secondary structure elements preformation is further supported by the utilization of the ^{15}N transversal relaxation rates (R_2) of the backbone amides. The R_2 values reveal three regions with higher R_2 relaxation rates that correspond to the three secondary structure elements in the region 50-100 (see Figure 1B). Residues located in the region comprising the α-helix have the highest R_2 values, as high as 8 s^{-1} at 18.8 T, as well as residues 86-100, which exhibit larger than average relaxation rates. Interestingly, the N-terminus (comprising the β-strand) and the linker region between the α-helix and Ω-loop have significantly lower values.

A comparison of the R_2 values and SSP scores with the disorder-probabilities (see Figure 2) computed by the deep neural network of ODiNPred (Dass et al., 2020) shows that based on the amino acid sequence of the protein one may expect ordered structures up to residues 72-75 that correspond to the C-terminus of the α-helix. Interestingly, residues 86-100 comprising the Ω-loop region exhibit a significantly increased disorder-probability. The disorder-probabilities' of residues 101-171 are on average >0.8 and are, therefore, in agreement with the experimental observations.

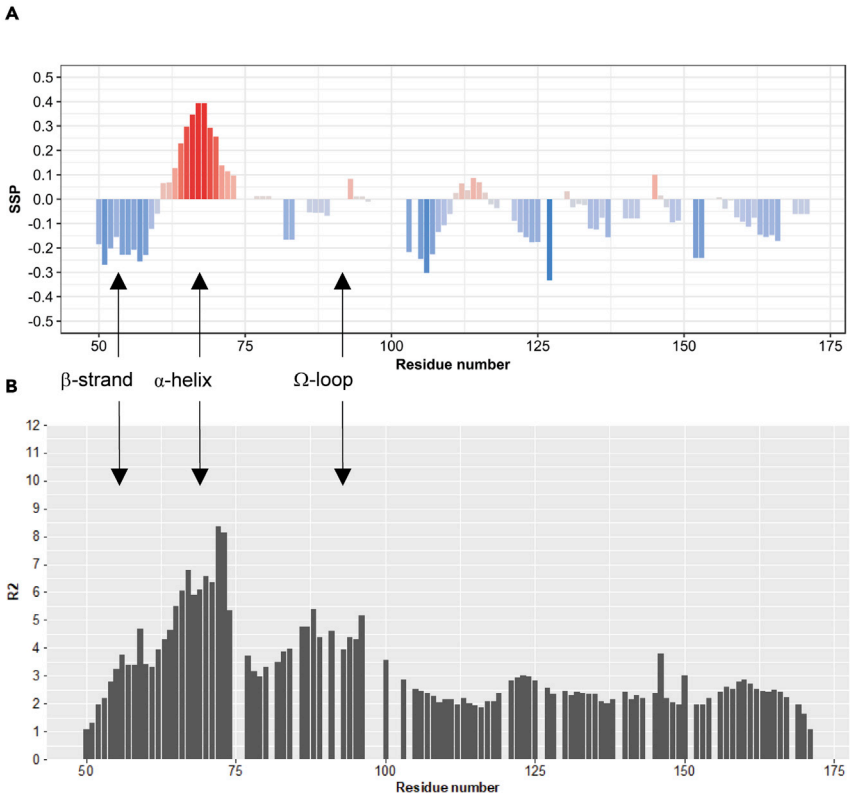

Figure 1. Chemical shift and relaxation data indicate preformation of secondary structure elements in the apo form of YAP

(A) SSP score (Marsh et al., 2006) of YAP^{wt} at pH 6 and 298 K. Positive scores indicate a propensity for α-helical structures, whereas β-strands or extended structural elements possess a negative score. SSP scores are not applicable to non-canonical secondary structure elements like the Ω-loop.

(B) ^{15}N R_2 Rates of YAP^{wt} at pH 6 and 298 K.

The detection of structural preformation within the Ω-loop region mandated another strategy as the SSP score is not applicable on non-canonical secondary structure elements like an Ω-loop. However, the R_2 values indicated the prevalence of slower dynamics in this region. Therefore, we used selective side-chain labeling with late metabolic precursors to identify long-range contacts (between residues separated by up to 10 residues in the primary sequence) that indicate the structural preformation of the Ω-loop region (Schörghuber et al., 2018). Based on the information from the crystal structure (Li et al., 2010) and the available biochemical data on the YAP:TEAD interaction (Mesrouze et al., 2017), we decided to specifically label methionine, leucine, and phenylalanine residues. Significant long-range side-chain NOEs between F95/96-H^{ζ}, M86-H^{ε}, and L91-H^{δ} were obtained (see Figure 3).

It was not possible to properly distinguish between F95 and F96 as the mutation of each one of these residues leads to major changes in the ^{1}H-^{13}C HSQC spectrum of the phenylalanine $^{1}H^{\zeta}$s (see Figure S1). However, the significant changes provide evidence for the formation of a compact state displaying distinct structural features. As can be seen in Figure 2, residues M86, L91, F95, and F96 show specific long-range NOEs which are in very good agreement with the geometry of the Ω-loop region in the final YAP:TEAD complex (Figure 2B). It can thus be concluded that a structure that resembles the hydrophobic core of the bound Ω-loop region already exists in the apo-state of YAP prior to TEAD binding.

Secondary structure element preformation is co-dependent

To provide additional information about this compact state we studied YAP mutants that were previously reported to have a major impact on the formation of the YAP:TEAD complex (Mesrouze et al., 2017). Most importantly, the α-helical propensity is consistently decreased in the different mutants. To visualize the

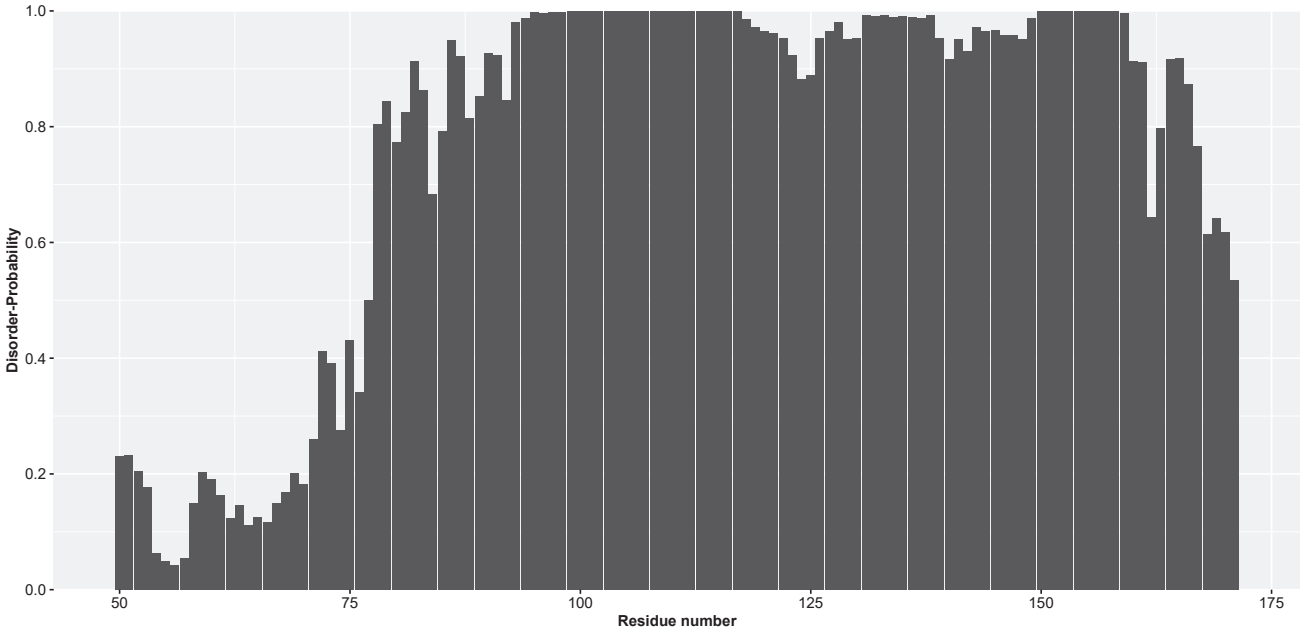

Figure 2. Disorder-probabilities of the YAP^{wt} amino acid sequence calculated via ODiNPred

change in secondary structure formation ΔSSP (SSP$_{wt}$ – SSP$_{mutant}$) were calculated (see Figure 4). Although this decrease in the helical propensity is expected for the mutation of residues located in the local LxxLF motif within the α-helix (L65A, L68A, F69A), the decrease of the helical propensity on the introduction of mutations within the Ω-loop region (M86A, R89A, L91A, F95A, F96A) more than 10 residues apart from the α-helix is rather surprising. These findings indicate that a destabilization of the Ω-loop structure through the mutation of crucial hydrophobic residues (M86A, L91A, F95A, F95A) that compose the hydrophobic core of the Ω-loop concurrently destabilizes the α-helical structure and decreases the helical population. In addition, the negatively charged R89 at the N-terminus of the Ω-loop also leads to a decrease of the helical propensity which might be the consequence of the disruption of the electrostatic interaction of this region with the positively charged C-terminus of the α-helix (Mesrouze et al., 2021). Interestingly, mutations that lead to more pronounced changes in the binding affinity of the YAP:TEAD complex (R89A, L91A, F95A, F96A) exhibit higher ΔSSP-values in the α-helical region. In addition, the propensity for an extended structure also decreases in the N-terminal β-strand region for all mutants except for L68A. This might be further supporting the notion that also the N-terminal extended structure that corresponds to β-strand region in the bound state undergoes some change on the introduction of these point mutations. Therefore, one can draw the hypothesis that the preformation of the extended structure at the N-terminus, α-helix, and Ω-loop are co-dependent. These results demand a more detailed investigation of the change in the long-range backbone dynamics within this N-terminal region of YAP^{wt}.

Long-range structural compaction of YAP^{wt}

Paramagnetic relaxation enhancement (PRE), which is one of the most relevant experimental approaches to probe for transient long-range contacts in IDPs (Kosen, 1989), was applied to YAP^{wt}. The presence of a paramagnetic (1-oxyl-2,2,5,5-tetramethyl-Δ3-pyrroline-3-methyl) methanethio-sulfonat (MTSL) spin label that is introduced at several protein positions leads to an enhancement of the transverse relaxation rates R_2 depending on the inverse sixth power of the distance ($1/r^6$) between the unpaired electron and the observed nucleus of the backbone amide hydrogen. To obtain a sufficient resolution (Silvestre-Ryan et al., 2013) of the whole protein fragment, 12 cysteines were introduced via site-directed mutagenesis at different positions: D60, A71, V80, K90, S103, T119, S127, S138, S149, Q158, S164, 172 (insertion). To determine if these mutations affect the YAP:TEAD interaction, the potency (IC_{50}) of the mutants was measured in a TR-FRET assay where one looks for their ability to compete with a Cy5-labelled version of YAP for binding to TEAD (Bokhovchuk et al., 2020b). The IC_{50} of the mutants is similar to the one obtained with YAP^{wt}, indicating that the mutations have no significant effect on their ability to bind to TEAD (see

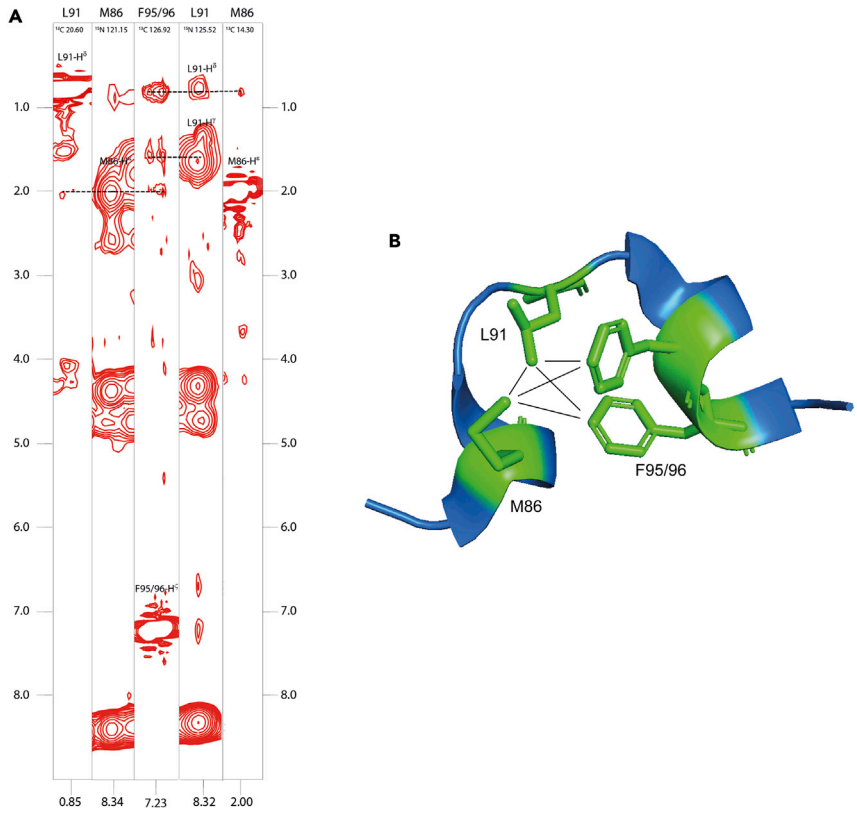

Figure 3. Structural preformation of the Ω-loop in YAP

(A) ^{13}C-NOESY-HSQC and ^{15}N-NOESY-HSQC strips demonstrating the close spatial proximity of the side chains of residues M86, L91, F95/96.

(B) Depiction of the NOE contacts observed in the apo form of YAP (dashed lines) in the crystal structure of the YAP:TEAD complex (PDB: 3KYS).

Table S1). Intermolecular PRE effects were excluded by control measurements of mixtures (1:1) of ^{15}N-labeled YAP^{wt} and ^{14}N MTSL-labeled YAP mutants. For this purpose, rates were measured for mixtures containing the ^{14}N MTSL-labeled mutants D60C, S103C, and S164C. The evaluation of all of them showed no significant PRE effects at the ^{15}N labeled backbone of YAP^{wt}. Therefore, intermolecular PRE effects can be excluded.

Inspection of Figure 5 provides strong evidence for the formation of compact states in YAP prior to TEAD binding. In particular, when the spin label is placed at positions 60 or 71, almost complete loss of signals is observed for residues of the N-terminus of YAP^{wt} (residues 50-100) owing to efficient paramagnetic relaxation induced by the spin label. In a similar manner, the MTSL spin label at position 90 leads to fast relaxation in the protein region from 65 to 100. The mutation at V80C is located in the loop region connecting the α-helix and Ω-loop in the known crystal structures. In contrast to the labels at position 60 or 71, the spin label attached to position 80 exhibits way fewer long-range backbone interactions than the three aforementioned positions. The data from the first four spin labels suggest a very close spatial proximity of the β-strand region, α-helix, and Ω-loop regions. In particular, the complete loss of the signal over a large region of the protein (~50 residues) upon the introduction of a spin label in the area of these secondary structure elements supports this hypothesis. Interestingly, higher PRE rates for the first 50 N-terminal residues were also observed for other spin label positions. This observation provides further support for the apparent compaction of the N-terminal segment and even suggests the global compaction of YAP in its apo-state.

As the PRE data provided evidence for a compacted state, we employed the recently introduced correlation matrix analysis of PRE data (see Figure 6). In previous publications, we demonstrated that this

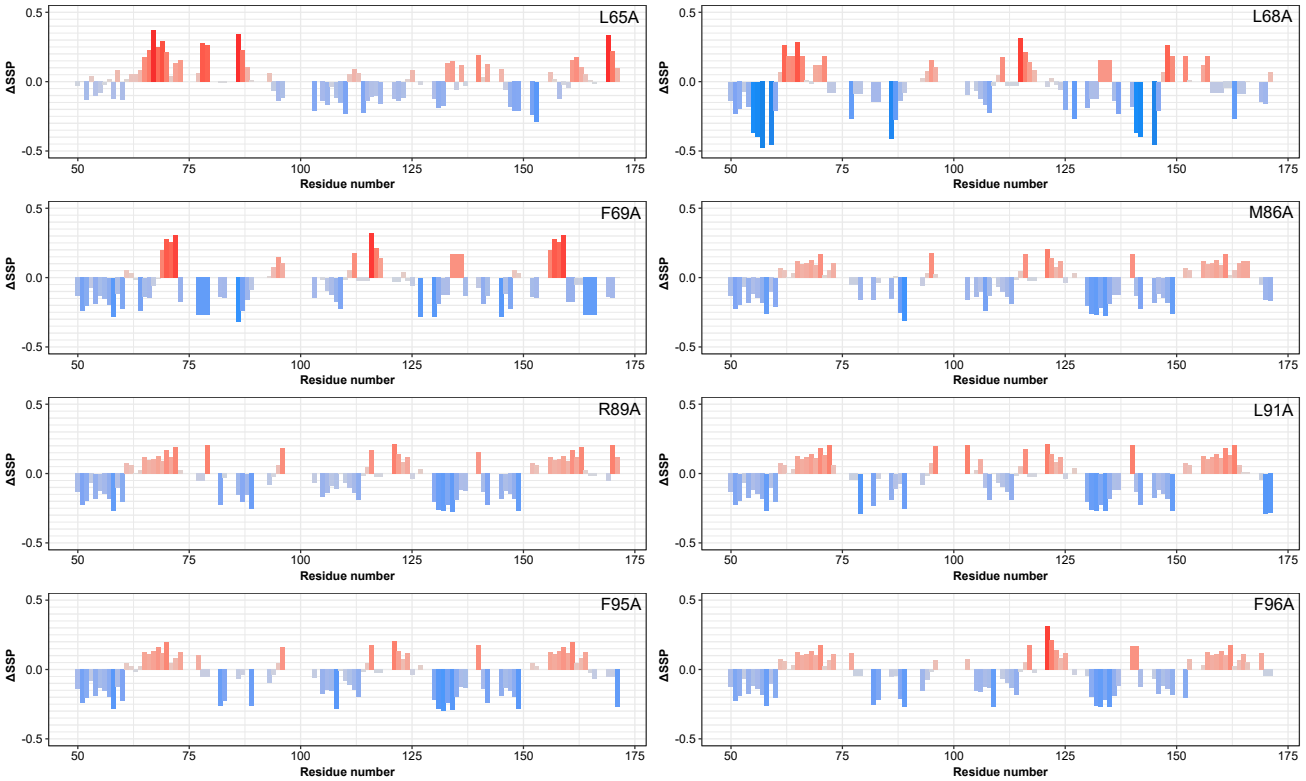

Figure 4. Preformation of secondary structure elements is interdependent

ΔSSP ($SSP_{wt} - SSP_{mutant}$) scores demonstrate the relative change in secondary structure propensity upon the introduction of point mutations. Higher values indicate higher deviations from the YAP^{wt} SSP scores.

approach yields unique insight into the conformational ensemble and concerted structural fluctuations of IDPs (Kurzbach et al., 2017). By applying this methodology to YAP, we are able to identify three regions that may exhibit structural compaction. The first region (I) between residues 50-100 corresponds to the TEAD binding interface identified in the crystal structure. The second positively correlated region around residue 127 (II) corresponds to the 14-3-3 binding site that is phosphorylated for the cytoplasmic retention of YAP. In addition, there seems to be some compaction in the C-terminus of the YAP fragment (III).

To further compare the degree of "compactness" of the structural ensemble in the apo state in comparison to the bound state, PRE rates were calculated *in silico* from the existing crystal structure (Li et al., 2010). The comparison of experimentally derived PRE rates and PRE rates calculated from the crystal structure suggests that the region between residues 50-100 adopts a structural conformation that may be described as even more compact than the conformation in the bound form (see Figure 7). PRE rates from the crystal structure were calculated under the assumption that in the bound state, the three secondary structure elements of YAP remain relatively rigid and have a well-defined structure. In addition, PRE rates >60 s^{-1} were excluded from the comparison as they were not detectable in our experimental setup. The comparison of the rates obtained for the spin label at position 80 shows that the spatial distance between the loop region and the α-helix increases in the apo state. This indicates a compensation mechanism for the close spatial proximity of the α-helix and Ω-loop in the apo state that sequesters the loop region further away from the α-helix in comparison to the bound state. Only the N-terminal β-strand region seems to be more rigid in the bound state, presumably owing to stabilizing interactions across the interface.

Yes-associated protein compaction has a kinetic contribution to the YAP:TEAD formation

To study the impact of the aforementioned mutations on the YAP:TEAD complex formation double mutants were produced that contained the reported mutations and the A71C spin labeling site. Interestingly, the degree of compaction has decreased in all mutated forms of YAP (see Figure 8). Figure 8 shows

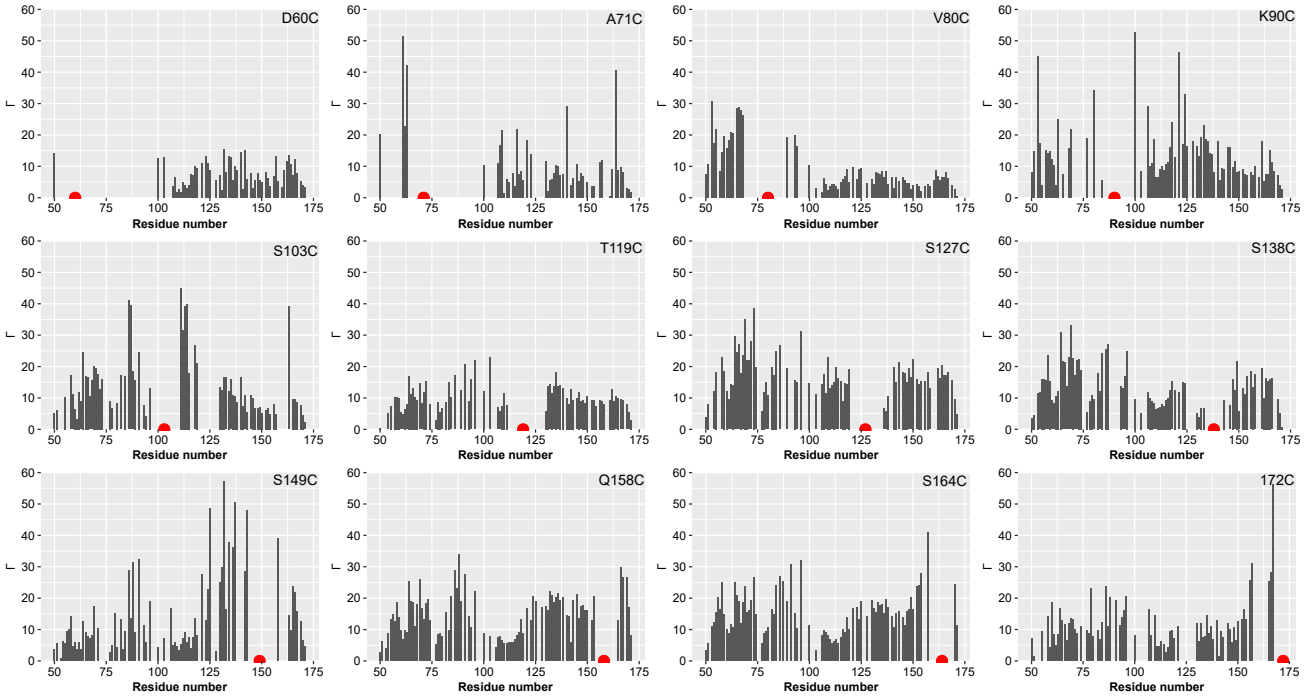

Figure 5. Long-range contacts in apo YAP

PRE rates measured by the introduction of MTSL spin labels at 12 different positions indicated by the red dots. High rates indicate spatial proximity between the spin label and the protein residue.

differential intensity ratios of the para- and diamagnetic peak intensities of YAP^{wt} with the spin label at A71C and the respective mutations also containing the A71C label. PRE differences for residues located in the region 101-171 are insignificant and are thus not shown. Inspection of Figure 8 reveals that the biggest difference in the PRE profiles is observed for the mutation L68A, which is part of the LxxLF motif in the α-helix. Specifically, residues 93-96 located at the C-terminal part of the Ω-loop exhibit a sizeable increase in the intensity ratios indicative of distinct spatial separation between the α-helix and Ω-loop in the mutant. The mutations L65A, M86A, and L91A primarily exhibit changes within the Ω-loop region, while the mutation F95A affects the β-strand and α-helix region in a significant manner. To conclude, the differential PRE data are in very good agreement with the observed reduction of secondary structure formation in the mutant forms and provide additional experimental evidence for the compact apo-state of YAP^{wt}.

To further corroborate the expansion of the YAP conformational ensembles, diffusion-ordered spectroscopy (DOSY) measurements of different mutants were performed (see Table 1). To increase the sensitivity for changes in the N-terminal region of YAP, a new construct ranging from residue 50 to 103 was produced and mutated at the respective sites. A comparison of the ^{1}H-^{15}N HSQC spectra exhibited a nearly perfect overlay of all peaks in the 50-103 construct and YAP^{wt}. The truncation, therefore, does not induce any significant changes in the structural ensembles. Inspection of the DOSY values yields a similar picture as the PRE data. The mutations L68A and F95A that lead to higher degrees of decompaction show slower diffusion constants. The mutation of F69A has the strongest effect on the diffusion constant.

Previous studies have shown that the same mutations change the kinetics of the YAP:TEAD formation and decrease the value of the association rate, k_{on}, for the complex formation (Bokhovchuk et al., 2020b). Their Φ-value analysis revealed that the α-helix already exists in the encounter complex preceding complex formation. Interestingly, the Ω-loop mutations induce on average smaller changes of the diffusion constant than the ones in the α-helix, indicating that the α-helix site contributes more to the global compact of YAP^{wt} and may be kinetically favored if YAP in its apo-state is adopting a more compacted and, therefore, faster diffusing state.

In addition to previous publications, our results about the compaction of YAP in its apo form suggest that there is an additional conformational selection step of the YAP:TEAD binding process happening on a

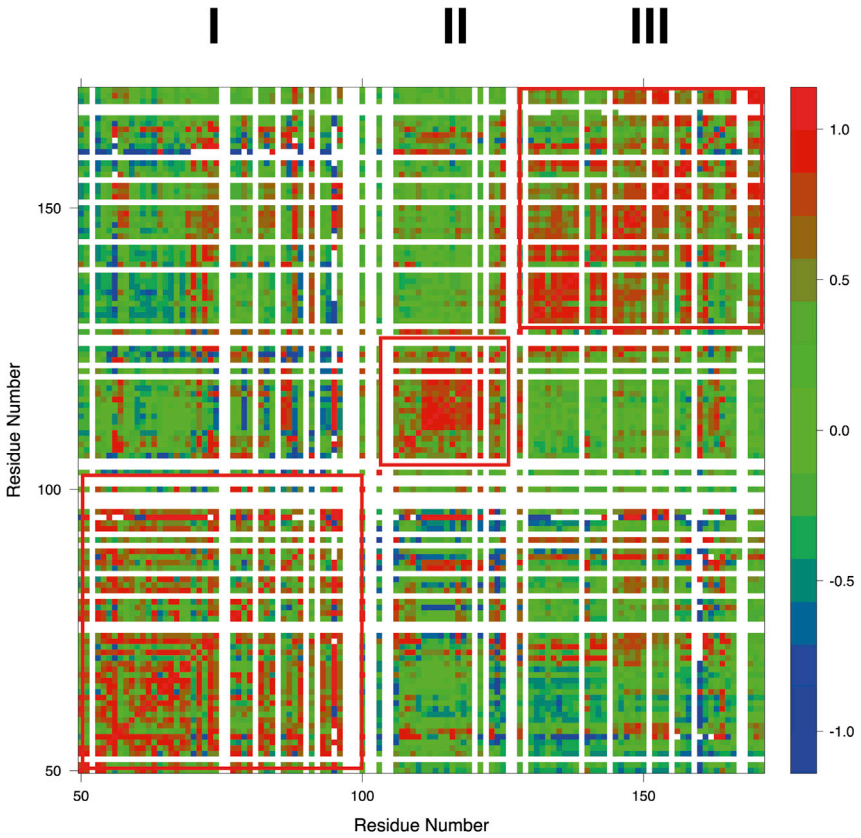

Figure 6. YAP exhibits three structurally correlated regions

Correlation analysis of PRE data obtained from 12 different spin labeling positions for YAP on pH 6 and 298 K. Positive correlations (red) indicate structurally correlated protein regions.

nanosecond timescale that could not be detected in previous stopped-flow experiments, but becomes clear through NMR. Thus, our NMR data again demonstrate the existence of a compact apo-state of YAP and its relevance for the formation of the encounter complex with TEAD.

DISCUSSION

Previous publications dissected and characterized the YAP:TEAD binding site (Chen et al., 2010; Hau et al., 2013; Li et al., 2010; Mesrouze et al., 2017) and provided a first glimpse on the mechanism of protein complex formation (Bokhovchuk et al., 2020b). However, structural information about the apo state of YAP and how putative structural preformation might influence its binding to TEAD has not yet been reported. The observed global compaction of apo YAP results from subtle and transient stabilizing interactions between localized secondary structures. In particular, the α-helical LxxLF (L65 to F69) motif and the Ω-loop region (M86 to F96) are crucial for the stabilization of a hydrophobic core resulting in the transient formation of a dynamic yet compact structure with distinct long-range correlations. Most importantly, these data are in very good agreement with prior mutational and kinetic studies that identified these residues as crucial for the nanomolar affinity between YAP and TEAD (Mesrouze et al., 2017) and, therefore, linking the preformation with the YAP:TEAD binding.

Surprisingly, the comparison of experimental PRE rates with predicted PRE rates obtained from the crystal structure of the YAP:TEAD complex revealed a structural arrangement in the apo form in which the secondary structure elements are already formed and even closer in space than in the bound form. In addition, we demonstrated that the C-terminal region outside the TEAD-binding domain also exhibits significant structural compaction. Interestingly, this region contains additional protein interaction sites (i.e. 14-3-3 binding site), and it seems plausible that these additional compaction "hot-spots" are relevant for YAP's biological

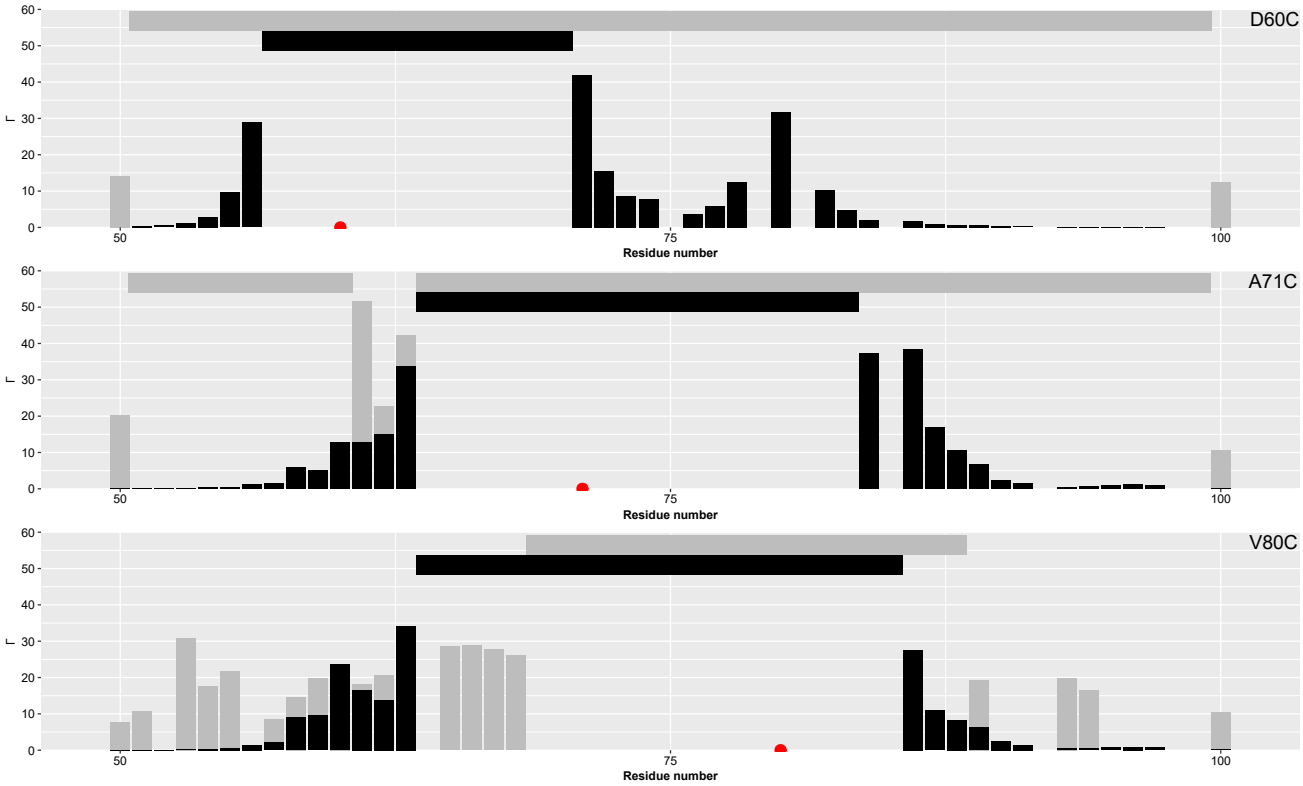

Figure 7. The TEAD-binding domain of YAP exhibits a structural ensemble that contains narrower spatial proximity than the one in the bound state

Comparison of experimentally derived (grey) and calculated PRE rates (black). The red dot indicates the position of the MTSL spin label. The horizontal bars indicate residue positions with no PRE value owing to relaxation rates that were not detectable in our experimental setup (grey) or calculated rates >60 s^{-1} that were excluded from the figure as they were not detectable in our experiments (black).

functionality by fine-tuning interaction networks with authentic partners. Transient intramolecular contacts between the individual subdomains in YAP might, therefore, provide a versatile and effective regulatory access control mechanism.

Using a combination of site-directed mutagenesis, ^{13}C chemical shifts, PRE measurements, and NMR-diffusion (DOSY) measurements, we could demonstrate that structural preformation and compaction in YAP is driven by the formation of a hydrophobic core established by residues from the previously described α-helix and Ω-loop. This is somewhat surprising as previous studies have shown that there is only a very weak correlation between increased hydrophobicity and structural compaction in IDPs. Marsh and Forman-Kay concluded that usually, the main facilitators of IDP compaction are net charge and proline content (Marsh and Forman-Kay, 2010). YAP, thereby, serves as an example for an IDP whose compaction is also driven by mechanisms reminiscent of folded (globular) proteins and thus questioning the conventional notion of IDPs being largely disordered. Furthermore, the formation of this hydrophobic core in YAP may be an example of the functional misfolding of an IDP to prevent unwanted interactions with non-native partners (Uversky, 2011). Uversky claims that there is chance that IDPs misfold to sequester the preformed elements inside the non-interactive or less-interactive cage as observable in the surprisingly compact apo state of YAP in which the interaction of the α-helix and Ω-loop may prevent their hydrophobic regions from unwanted interactions.

The observed structural compaction of apo YAP also provides a compelling structural explanation for the proposed mechanistic model of the YAP:TEAD complex formation (Bokhovchuk et al., 2020b). According to this study, the α-helix binding interface is formed at an earlier stage of the binding event, which is in good agreement with our data that show that mutations of the LxxLF motif of the α-helix have the biggest impact on the overall compaction of YAP and, thereby, may as well influence the binding kinetics. The initial α-helical preformation serves as a scaffold for the formation and, consequently, co-stabilization of the other two secondary structure elements. The resulting compact substrate allows for a rapid and efficient

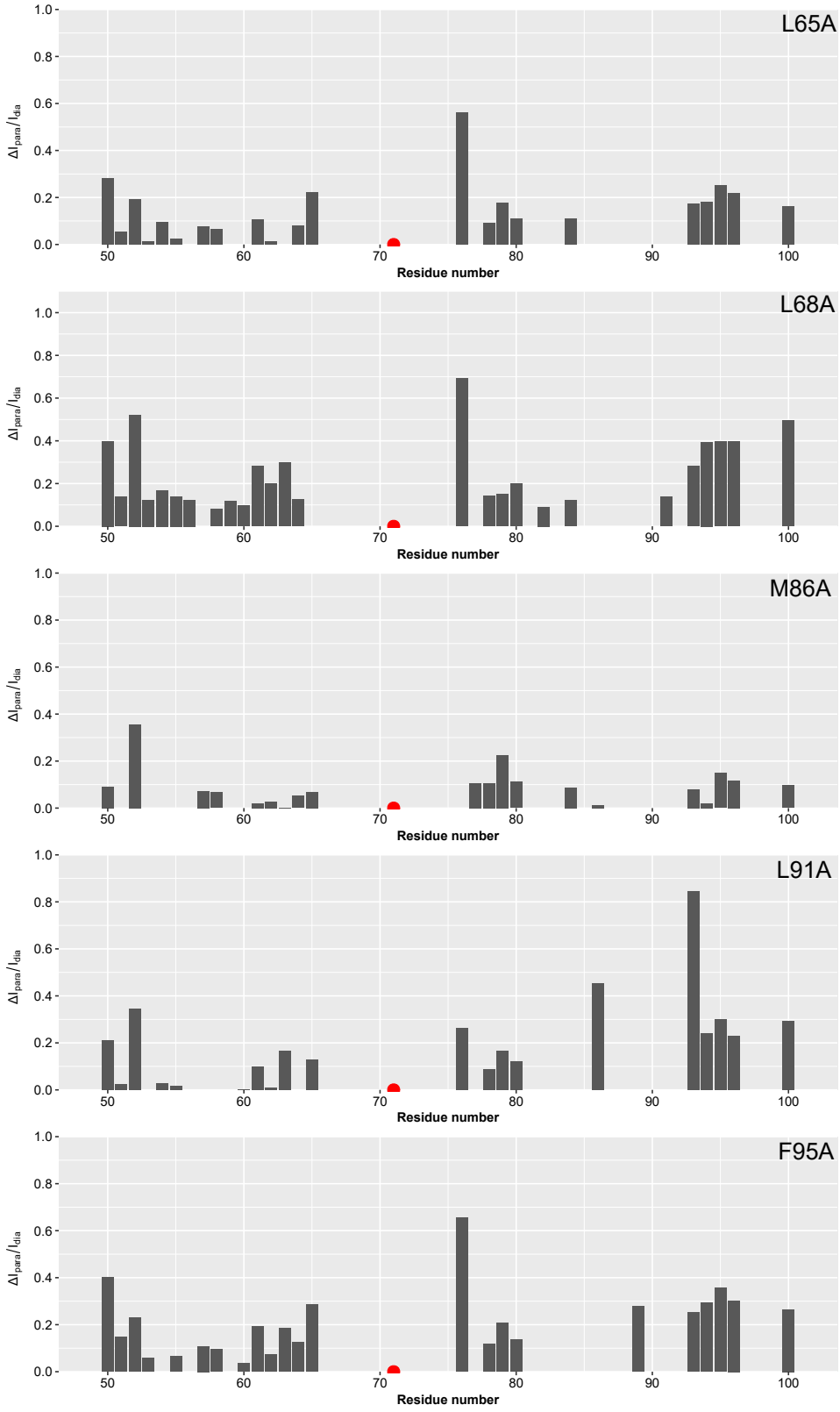
L65A
L68A
M86A
L91A
F95A
$\Delta I_{para}/I_{dia}$
1.0
0.8
0.6
0.4
0.2
0.0
50
60
70
80
90
100
Residue number

Figure 8. Long-range structural changes on the introduction of mutations
The differential between the intensity ratios of the para- and diamagnetic peak intensities of YAP^{wt} with the spin label at A71C and the respective mutations containing the same spin label. Higher values indicate an increase in the spatial proximity between the spin label and the residue position.

formation of a protein encounter complex that subsequently readjusts to the final shape. We thus propose that TEAD binding proceeds largely via conformational selection of the preformed compact substate that is happening on a nanosecond timescale and, therefore, was not detectable with previous methods applied to characterize the binding process.

The observation of long-range structural preformation in apo YAP also provides possible starting points for the inhibition of the YAP:TEAD interaction via targeting of the apo state of YAP as this may work with large hydrophobic molecules such as Verteporfin and hexasubstituted dipyrrins (Gibault et al., 2017) that seemingly inhibit the YAP:TEAD complex through YAP binding (Liu-chittenden et al., 2012). Such compounds may preferentially bind to the compact state (providing a characteristic arrangement of electrostatic and hydrophobic moieties) and might interfere with the co-stabilization function of the α-helix and Ω-loop and, hence, disrupt the compact state of YAP.

To conclude, the surprisingly compact state of apo YAP and its relevance for protein complex formation as well as inhibitory ligand binding illustrates the often neglected structural diversity of IDPs and the possibility to tackle these challenging targets by rational, structure-based approaches.

Limitations of the study

This study investigates the apo form of YAP^{wt} and the effect of mutations on the formation of local and global structured elements. However, the study was performed only with the TEAD-binding domain of YAP ranging from residues 50-171 and, we, therefore, did not analyze possible interactions between that fragment and other domains of YAP. Furthermore, analysis and mutation of some of the proline residues in YAP may allow further insights into the compaction of the apo state.

STAR★METHODS

Detailed methods are provided in the online version of this paper and include the following:

- KEY RESOURCES TABLE
- RESOURCE AVAILABILITY
  - Lead contact
  - Materials availability
  - Data and code availability
- METHOD DETAILS
  - Cloning
  - Site-directed mutagenesis
  - Protein expression and purification
  - MTSL tagging
  - Precursor labeling
  - TR-FRET
  - NMR spectroscopy
- QUANTIFICATION AND STATISTICAL ANALYSIS

Table 1. Kinetic effects of different YAP mutations visualized through diffusion coefficients (D)

	Mutation	D (10^{-11} m^2 s^{-1})
α-helix	wt	13.8 ± 0.1
	L68A	12.1 ± 0.1
	F69A	11.2 ± 0.1
Ω-loop	M86A	13.2 ± 0.1
	L91A	12.88 ± 0.02
	F95A	11.8 ± 0.1

SUPPLEMENTAL INFORMATION

Supplemental information can be found online at https://doi.org/10.1016/j.isci.2022.104099.

ACKNOWLEDGMENTS

The authors thank Georg Kontaxis for pulse sequence programming and general NMR expertise. Funding for the work was provided by Wiener Wissenschafts-, Forschungs- und Technologiefonds (WWTF), the Christian Doppler Laboratory for High-Content Structural Biology and Biotechnology, Austria and the Austrian Academy of Science (ÖAW) .

AUTHOR CONTRIBUTIONS

M.F. conceived and performed the experiments, and wrote the article. A.B. assisted in analyzing the data. M.M. and M.S. prepared and purified mutants. F.B. performed and analyzed the TR-FRET experiments. P.C. provided expertise and feedback. R.K. supervised the project, provided expertise and feedback, and secured funding.

DECLARATION OF INTERESTS

The authors declare no competing interests.

Received: October 14, 2021
Revised: January 25, 2022
Accepted: March 15, 2022
Published: April 15, 2022

REFERENCES

Bokhovchuk, F., Mesrouze, Y., Delaunay, C., Martin, T., Villard, F., Meyerhofer, M., Fontana, P., Zimmermann, C., Erdmann, D., Furet, P., et al. (2020a). Identification of FAM181A and FAM181B as new interactors with the TEAD transcription factors. Protein Sci. *29*, 509–520. https://doi.org/10.1002/pro.3775.

Bokhovchuk, F., Mesrouze, Y., Meyerhofer, M., Zimmermann, C., Fontana, P., Erdmann, D., Jemth, P., and Chène, P. (2020b). An early association between the α-helix of the TEAD binding domain of YAP and TEAD drives the formation of the YAP:TEAD complex. Biochemistry *59*, 1804–1812. https://doi.org/10.1021/acs.biochem.0c00217.

Calses, P.C., Crawford, J.J., Lill, J.R., and Dey, A. (2019). Hippo pathway in cancer: aberrant regulation and therapeutic opportunities. Trends Cancer *5*, 297–307. https://doi.org/10.1016/j.trecan.2019.04.001.

Carey, M.F., Peterson, C.L., and Smale, S.T. (2013). PCR-mediated site-directed mutagenesis. Cold Spring Harb. Protoc. *2013*, 738–742. https://doi.org/10.1101/pdb.prot076505.

Chen, L., Chan, S.W., Zhang, X., Walsh, M., and Lim, C.J. (2010). Structural basis of YAP recognition by TEAD4 in the Hippo pathway structural basis of YAP recognition by TEAD4 in the Hippo pathway. Genes Dev. *24*, 290–300. https://doi.org/10.1101/gad.1865310.

Crawford, J.J., Bronner, S.M., and Zbieg, J.R. (2018). Hippo pathway inhibition by blocking the YAP/TAZ–TEAD interface: a patent review. Expert Opin. Ther. Pat. *28*, 1–7. https://doi.org/10.1080/13543776.2018.1549226.

Dass, R., Mulder, F.A.A., and Nielsen, J.T. (2020). ODiNPred: comprehensive prediction of protein order and disorder. Sci. Rep. *10*, 1–16. https://doi.org/10.1038/s41598-020-71716-1.

Delaglio, F., Grzesiek, S., Vuister, G.W., Zhu, G., Pfeifer, J., and Bax, A. (1995). NMRPipe: a multidimensional spectral processing system based on UNIX pipes. J. Biomol. NMR *6*, 277–293. https://doi.org/10.1007/BF00197809.

Feichtinger, M., Sára, T., Platzer, G., Mateos, B., Bokhovchuk, F., Chène, P., and Konrat, R. (2018). 1H, 13C, 15N resonance assignment of human YAP 50–171 fragment. Biomol. NMR Assign. *12*, 179–182. https://doi.org/10.1007/s12104-018-9805-8.

Gibault, F., Bailly, F., Corvaisier, M., Coevoet, M., Huet, G., Melnyk, P., and Cotelle, P. (2017). Molecular features of the YAP inhibitor Verteporfin: synthesis of hexasubstituted dipyrrins as potential inhibitors of YAP/TAZ, the downstream effectors of the Hippo pathway. ChemMedChem *12*, 954–961. https://doi.org/10.1002/cmdc.201700063.

Goddard, T.D., and Kneller, D.G. (2004). SPARKY *314* (University California), p. 15.

Hau, J.C., Erdmann, D., Mesrouze, Y., Furet, P., Fontana, P., Zimmermann, C., Schmelzle, T., Hofmann, F., and Chène, P. (2013). The TEAD4-YAP/TAZ protein-protein interaction: expected similarities and unexpected differences. ChemBioChem *14*, 1218–1225.

Holden, J.K., and Cunningham, C.N. (2018). Targeting the Hippo pathway and cancer through the TEAD family of transcription factors. Cancers (Basel) *10*, 81. https://doi.org/10.3390/cancers10030081.

Klopp, J., Winterhalter, A., Gébleux, R., Scherer-becker, D., Ostermeier, C., and Alvar Gossert, D. (2018). Cost-effective large-scale expression of proteins for NMR studies. J. Biomol. NMR *71*, 247–262. https://doi.org/10.1007/s10858-018-0179-0.

Kosen, P.A. (1989). Spin labeling of proteins. Methods Enzymol. *177*, 86–121. https://doi.org/10.1016/0076-6879(89)77007-5.

Kurzbach, D., Beier, A., Vanas, A., Flamm, A.G., Platzer, G., Schwarz, T.C., and Konrat, R. (2017). NMR probing and visualization of correlated structural fluctuations in intrinsically disordered proteins. Phys. Chem. Chem. Phys. *19*, 10651–10656. https://doi.org/10.1039/C7CP00430C.

Li, Z., Zhao, B., Wang, P., Chen, F., Dong, Z., and Yang, H. (2010). Structural insights into the YAP and TEAD complex service Structural insights into the YAP and TEAD complex. Genes Dev. *24*, 235–240. https://doi.org/10.1101/gad.1865810.

Lichtenecker, R.J., Coudevylle, N., Konrat, R., and Schmid, W. (2013a). Selective Isotope labelling of leucine residues by using α-ketoacid precursor compounds. ChemBioChem *14*, 818–821. https://doi.org/10.1002/cbic.201200737.

Lichtenecker, R.J., Weinhäupl, K., Schmid, W., and Konrat, R. (2013b). α-Ketoacids as precursors for phenylalanine and tyrosine labelling in cell-based protein overexpression. J. Biomol. NMR *57*, 327–331. https://doi.org/10.1007/s10858-013-9796-9.

Liu-chittenden, Y., Huang, B., Shim, J.S., Chen, Q., Lee, S., Anders, R.A., Liu, J.O., and Pan, D. (2012). Genetic and pharmacological disruption of the TEAD–YAP complex suppresses the

oncogenic activity of YAP. Genes Dev. *26*, 1300–1305. https://doi.org/10.1101/gad.192856.112.

Liu, A.M., Wong, K.F., Jiang, X., Qiao, Y., and Luk, J.M. (2012). Regulators of mammalian Hippo pathway in cancer. Biochim. Biophys. Acta *1826*, 357–364. https://doi.org/10.1016/j.bbcan.2012.05.006.

Ma, S., Meng, Z., Chen, R., and Guan, K.-L. (2019). The Hippo pathway: biology and pathophysiology. Annu. Rev. Biochem. *88*, 577–604. https://doi.org/10.1146/annurev-biochem-013118-111829.

Ma, Y., Yang, Y., Wang, F., Wei, Q., and Qin, H. (2015). Hippo-YAP signaling pathway: a new paradigm for cancer therapy. Int. J. Cancer *137*, 2275–2286. https://doi.org/10.1002/ijc.29073.

Marley, J., Lu, M., and Bracken, C. (2001). A method for efficient isotopic labeling of recombinant proteins. J. Biomol. NMR *20*, 71–75. https://doi.org/10.1023/A:1011254402785.

Marsh, J.A., Singh, V.K., Jia, Z., and Forman-Kay, J.D. (2006). Sensitivity of secondary structure propensities to sequence differences between alpha- and gamma-synuclein: implications for fibrillation. Protein Sci. *15*, 2795–2804. https://doi.org/10.1110/ps.062465306.

Marsh, J.A., and Forman-Kay, J.D. (2010). Sequence determinants of compaction in intrinsically disordered proteins. Biophys. J. *98*, 2374–2382. https://doi.org/10.1016/j.bpj.2010.02.012.

Mesrouze, Y., Bokhovchuk, F., Meyerhofer, M., Fontana, P., Zimmermann, C., Martin, T., Delaunay, C., Erdmann, D., Schmelzle, T., and Chène, P. (2017). Dissection of the interaction between the intrinsically disordered YAP protein and the transcription factor TEAD. Elife *6*, 1–16. https://doi.org/10.7554/eLife.25068.001.

Mesrouze, Y., Bokhovchuk, F., Meyerhofer, M., Zimmermann, C., Fontana, P., Erdmann, D., and Chène, P. (2021). Study of the TEAD-binding domain of the YAP protein from animal species. Protein Sci. *30*, 339–349. https://doi.org/10.1002/pro.3988.

Moya, I.M., and Halder, G. (2019). Hippo–YAP/TAZ signalling in organ regeneration and regenerative medicine. Nat. Rev. Mol. Cell Biol. *20*, 211–226. https://doi.org/10.1038/s41580-018-0086-y.

Pobbati, A.V., Han, X., Hung, A.W., Weiguang, S., Huda, N., Chen, G.Y., Kang, C.B., Chia, C.S.B., Luo, X., Hong, W., and Poulsen, A. (2015). Targeting the central pocket in human transcription factor TEAD as a potential cancer therapeutic strategy. Structure *23*, 2076–2086. https://doi.org/10.1016/j.str.2015.09.009.

Pobbati, A.V., and Hong, W. (2013). Emerging roles of TEAD transcription factors and its coactivators in cancers. Cancer Biol. Ther. *14*, 390–398. https://doi.org/10.4161/cbt.23788.

RStudio Team (2017). RStudio: Integrated Development for R (RStudio, Inc.). https://doi.org/10.1007/978-81-322-2340-5. http//www.rstudio.com.

Santucci, M., Vignudelli, T., Ferrari, S., Mor, M., Scalvini, L., Bolognesi, M.L., Uliassi, E., and Costi, M.P. (2015). The Hippo pathway and YAP/TAZ-TEAD protein-protein interaction as targets for regenerative medicine and cancer treatment. J. Med. Chem. *58*, 4857–4873. https://doi.org/10.1021/jm501615v.

Scholz, J., Besir, H., Strasser, C., and Suppmann, S. (2013). A new method to customize protein expression vectors for fast, efficient and background free parallel cloning. BMC Biotechnol. *13*, 12. https://doi.org/10.1186/1472-6750-13-12.

Schörghuber, J., Geist, L., Platzer, G., Feichtinger, M., Bisaccia, M., Scheibelberger, L., Weber, F., Konrat, R., and Lichtenecker, R.J. (2018). Late metabolic precursors for selective aromatic residue labeling. J. Biomol. NMR *71*, 129–140. https://doi.org/10.1007/s10858-018-0188-z.

Silvestre-Ryan, J., Bertoncini, C.W., Fenwick, R.B., Esteban-Martin, S., and Salvatella, X. (2013). Average conformations determined from PRE data provide high-resolution maps of transient tertiary interactions in disordered proteins. Biophys. J. *104*, 1740–1751. https://doi.org/10.1016/j.bpj.2013.02.019.

Tian, W., Yu, J., Tomchick, D.R., Pan, D., and Luo, X. (2010). Structural and functional analysis of the YAP-binding domain of human TEAD2. Proc. Natl. Acad. Sci. U S A *107*, 7293–7298. https://doi.org/10.1073/pnas.1000293107.

Tremblay, A.M., and Camargo, F.D. (2012). Hippo signaling in mammalian stem cells. Semin. Cell Dev. Biol. *23*, 818–826. https://doi.org/10.1016/j.semcdb.2012.08.001.

Uversky, V.N. (2011). Intrinsically disordered proteins may escape unwanted interactions via functional misfolding. Biochim. Biophys. Acta *1814*, 693–712. https://doi.org/10.1016/j.bbapap.2011.03.010.

Vassilev, A., Kaneko, K.J., Shu, H., Zhao, Y., and Depamphilis, M.L. (2001). YAP65 , a Src/Yes-associated protein localized in the cytoplasm TEAD/TEF transcription factors utilize the activation domain of YAP65 , a Src/Yes-associated protein localized in the cytoplasm. Genes Dev. *15*, 1229–1241. https://doi.org/10.1101/gad.888601.

Vranken, W.F., Boucher, W., Stevens, T.J., Fogh, R.H., Pajon, A., Llinas, M., Ulrich, E.L., Markley, J.L., Ionides, J., and Laue, E.D. (2005). The CCPN data model for NMR spectroscopy: development of a software pipeline. Proteins *59*, 687–696. https://doi.org/10.1002/prot.20449.

Wang, Y., Yu, A., and Yu, F.X. (2017). The Hippo pathway in tissue homeostasis and regeneration. Protein Cell *8*, 349–359. https://doi.org/10.1007/s13238-017-0371-0.

Ye, S., and Eisinger-Mathason, T.S.K. (2016). Targeting the Hippo pathway: clinical implications and therapeutics. Pharmacol. Res. *103*, 270–278. https://doi.org/10.1016/j.phrs.2015.11.025.

Zhao, B., Zhao, B., Wei, X., Wei, X., Li, W., Li, W., Udan, R.S., Udan, R.S., Yang, Q., Yang, Q., et al. (2007). Inactivation of YAP oncoprotein by the Hippo pathway is involved in cell contact inhibition and tissue growth control. Genes Dev. *21*, 2747–2761. https://doi.org/10.1101/gad.1602907.Hpo/Sav.

Zhao, B., Tumaneng, K., and Guan, K.L. (2011). The Hippo pathway in organ size control, tissue regeneration and stem cell self-renewal. Nat. Cell Biol. *13*, 877–883. https://doi.org/10.1038/ncb2303.

STAR★METHODS

KEY RESOURCES TABLE

REAGENT or RESOURCE	SOURCE	IDENTIFIER
Bacterial and virus strains		
E. coli TOP10	Thermo Fisher	Cat#C404010
E. coli Tuner™(DE3)	Sigma-Aldrich	Cat#70625
Chemicals, peptides, and recombinant proteins		
YAP^{50-171}	Produced by authors	N/A
YAP^{50-103}	Produced by authors	N/A
DpnI	Thermo Fisher	Cat#ER1701
recA	Thermo Fisher	Cat#RP-4900
^{15}N ammonium chloride	Sigma-Aldrich	Cat#299251
^{13}C glucose	Cambridge Isotopes	Cat#CLM-1396
Protease Inhibitor Cocktail	Thermo Fisher	Cat#78429
L-Methionin-(*methyl*-^{13}C)	Sigma-Aldrich	Cat#299146
Isotopically labeled Phenylalanine precursor	Produced by Group Lichtenecker, University of Vienna	N/A
Isotopically labeled Leucine precursor	Produced by Group Lichtenecker, University of Vienna	N/A
(1-oxyl-2,2,5,5-tetramethyl-Δ3-pyrroline-3-methyl) methanethio-sulfonat (MTSL)	Sigma-Aldrich	Cat#81213
Critical commercial assays		
Phusion Flash PCR Master Mix	Thermo Fisher	Cat#F548L
Oligonucleotides		
Oligonucleotides for PCR-mediated mutagenesis of various YAP mutants	See Table S2 for a list of oligonucleotides	N/A
Recombinant DNA		
pEtM14 vector containing YAP fusion protein with His6-tag and 3 C cleavage site	Produced by authors	N/A
Software and algorithms		
NMRPipe	Delaglio et al., 1995	https://www.ibbr.umd.edu/nmrpipe/
CcpNmr	Vranken et al., 2005	https://ccpn.ac.uk/
Sparky	Goddard and Kneller, 2004	https://www.cgl.ucsf.edu/home/sparky/
RStudio	RStudio Team	https://www.rstudio.com/

RESOURCE AVAILABILITY

Lead contact

Further information and requests for resources and reagents should be directed to and will be fulfilled by the lead contact, Michael Feichtinger (michael.feichtinger@univie.ac.at).

Materials availability

- A table containing all oligonucleotides (Table S2. Oligonucleotides used) in this work can be found in the supplemental information.
- All chemicals, plasmids, recombinant proteins, and software used are listed in the key resources table.

Data and code availability

- All data reported in this paper will be shared by the lead contact upon request.
- The data does not report original code.
- Any additional information required to reanalyze the data reported in this paper is available from the lead contact upon request.

METHOD DETAILS

Cloning

The sequence coding for YAP residues 50–171 was cloned into a pETM14 vector by Sequence and Ligation Independent Cloning (SLIC) (Scholz et al., 2013). Therefore, the coding sequence of YAP was amplified by polymerase chain reaction (PCR) using primers containing 25 bp overlapping homologies of the target vector at each end. The remaining copies of the initial template vector were removed by a 1-h digest with the restriction enzyme DPNI. An aliquot of approximately 100 ng of the PCR product (coding sequence of YAP 50–171) was mixed in a total volume of 10 μL with approximately 100 ng of the target pETM14 vector and recA; consequently, the mixture was incubated at 37°C for an additional hour. The recombinase recA recombines the PCR products into the target vector due to the overlapping homologous regions. The whole 10 μL were transformed into *E. coli* TOP10 cells and the resulting plasmids were evaluated by sequencing. The final pETM14 vector contained a YAP fusion protein with His6-tag and a 3 C protease cleavage site at the N-terminus.

Site-directed mutagenesis

For PCR-mediated mutagenesis, a single PCR step using full plasmid amplification was used (Carey et al., 2013). Hence, 0.2 μL of each 25 bp primer (concentration of 100 μM), 50 ng of plasmid DNA and 20 μL Phusion Flash PCR Master Mix (Thermo Fisher) were combined in a total volume of 40 μL. Then PCR was run for 20 cycles, each consisting of 30 s of denaturation at 96°C and of 2 min of elongation at 72°C. The remaining copies of the initial template vector were removed by a 1-h digest with the restriction enzyme DPNI. Afterwards, 2 μL of each PCR product were transformed into *E. coli* TOP10 cells and the resulting plasmids were evaluated by sequencing.

Protein expression and purification

The plasmid, containing the fusion protein with a His6-tag at the N-terminus and a 3C protease cleavage site, was transformed into *E. coli* Tuner™(DE3). Four liters of LB medium, supplemented with Kanamycin, were inoculated with the overnight culture and incubated at 37°C until an OD_{600} of 0.8. The cells were centrifuged and all the pellets were combined and resuspended in one liter of M9 minimal medium containing 1 g/L ^{15}N ammonium chloride (Sigma-Aldrich) and 3 g/L ^{13}C glucose (Cambridge Isotope) as the sole source of nitrogen and carbon, respectively (Marley et al., 2001). After an additional hour at 37°C, the expression was induced with the addition of 0.8 mM IPTG and cells were incubated for 18 h at 30°C and consecutively harvested by centrifugation and stored at −20°C.

Frozen cell pellets were resuspended in lysis buffer (20 mM Tris, 150 mM NaCl, 30 mM Imidazole, pH 7.8), supplemented with 50 μL of Protease Inhibitor Cocktail (Thermo Scientific), and lysed by sonication on ice. The lysate was clarified by centrifugation and the supernatant was loaded onto a HisTrap FF column and washed with 8 column volumes of wash buffer (20 mM Tris, 150 mM NaCl, 40 mM Imidazole, pH 7.8). After eluting with 15 mL of elution buffer (20 mM Tris, 150 mM NaCl, 300 mM Imidazole, 1 mM EDTA, pH 7.8), the eluate was concentrated to 2 mL and dialyzed overnight against an excess of NMR buffer (20 mM BisTris, 150 mM NaCl, 1 mM EDTA, pH 6.0). Consequently, the His6-tag was removed by 3C protease cleavage overnight at 4°C. NaCl was added to the final concentration of 1 M and the solution was heated to 90°C for 10 min. After centrifugation, the supernatant was loaded onto a HiLoad 16/600 (GE Healthcare) size exclusion column, equilibrated with the NMR buffer. Fractions containing the protein were pooled and concentrated. In the case of the Cysteine mutants, all the buffers were supplemented with 1 mM DTT.

Purified protein, which was >95% pure as assessed by SDS/PAGE (see Figures 2, 3, and 4), was concentrated to approximately 0.5 mM in the NMR buffer containing 10% D_2O. Owing to the lack of absorbance at 280 nm, the protein concentration was determined by the Pierce BCA Protein Assay (Thermo Scientific).

MTSL tagging

The MTSL tagging was initiated combining 1 mL of protein solution with 1 mL of MTSL reaction buffer (100 mM NaP, 1 mM EDTA, pH 8.0) and by incubating it at RT for 15 min after the addition of a 10-fold excess (in comparison to the protein concentration) of DTT. This ensures that all the Cysteines are reduced for the MTSL-tagging procedure. Afterwards, DTT was removed by the PD-10 desalting column and the protein solution was eluted in 3.3 mL of MTSL reaction buffer. From a 50 mM DMSO stock solution, two times excess of MTSL was added to the protein solution. Consequently, the protein solution containing MTSL was incubated for 3 h at 30°C with agitation. Finally, the free MTSL was removed and the sample concentrated by exchange with the NMR Buffer via a Amicon Centricon MWCO 3 kDa. For the measurement of the diamagnetic control experiments, the free electron of the MTSL tag was reduced by a two-fold excess of ascorbic acid.

Precursor labeling

The precursor labeling was done by the addition of 1 g/L of $^{13}C^{\varepsilon}$-methionine (Sigma-Aldrich) and 10 mg/mL of the isotopically labeled phenylalanine and leucine precursors to the M9 minimal medium used for protein expression (Klopp et al., 2018; Lichtenecker et al., 2013a, 2013b).

TR-FRET

Biotinylated N-Avitagged-TEAD4$^{217–434}$ (1 nM) and LANCE Eu-W1024 Streptavidin (0.5 nM, PerkinElmer) were pre-incubated for 1 h at room temperature in 50 mM HEPES pH 7.4, 100 mM KCl, 0.05% (v/v) Tween-20, 0.25 mM TCEP, 1 mM, and 0.05% (w/v) BSA. Different YAP mutants (20 nM) and serial dilutions of them were added and incubated in white 384-well plates (Greiner Bio-One International) for 1 h at room temperature. DMSO was present at 2% in the assay. The solubility of the peptides in assay buffer was measured by dynamic light scattering with a Dyna Protdevice (Wyatt technology Corp.). The fluorescence in the TR- FRET assay was measured with a Genios Pro reader (Tecan) (50 μs delay between excitation and fluores- cence, 75 μs integration time, excitation wavelength 340 nm, emission wavelengths 620 and 665 nm). Data analyses were carried out using the TR-FRET 665/620 nm emission ratio. The IC_{50} values were obtained by nonlinear regression analysis with GraphPad Prism (GraphPad Software) (Bokhovchuk et al., 2020a).

NMR spectroscopy

NMR experiments were performed at 298 K using a Bruker Avance III 800 MHz, Bruker Neo 600 MHz, and Bruker Neo 500 MHz spectrometer. Data were processed using NMRPipe (Delaglio et al., 1995) and Bruker TopSpin. Spectra were analyzed using CcpNmr (Vranken et al., 2005) and Sparky (Goddard and Kneller, 2004). Further data analysis and plots were performed and created, respectively, with RStudio (RStudio Team, 2017).

QUANTIFICATION AND STATISTICAL ANALYSIS

The IC_{50} values were obtained by nonlinear regression analysis with GraphPad Prism (Table S1).

iScience, Volume *25*

Supplemental information

Long-range structural preformation in yes-associated protein precedes encounter complex formation with TEAD

Michael Feichtinger, Andreas Beier, Mario Migotti, Matthias Schmid, Fedir Bokhovchuk, Patrick Chène, and Robert Konrat

Supplemental Information

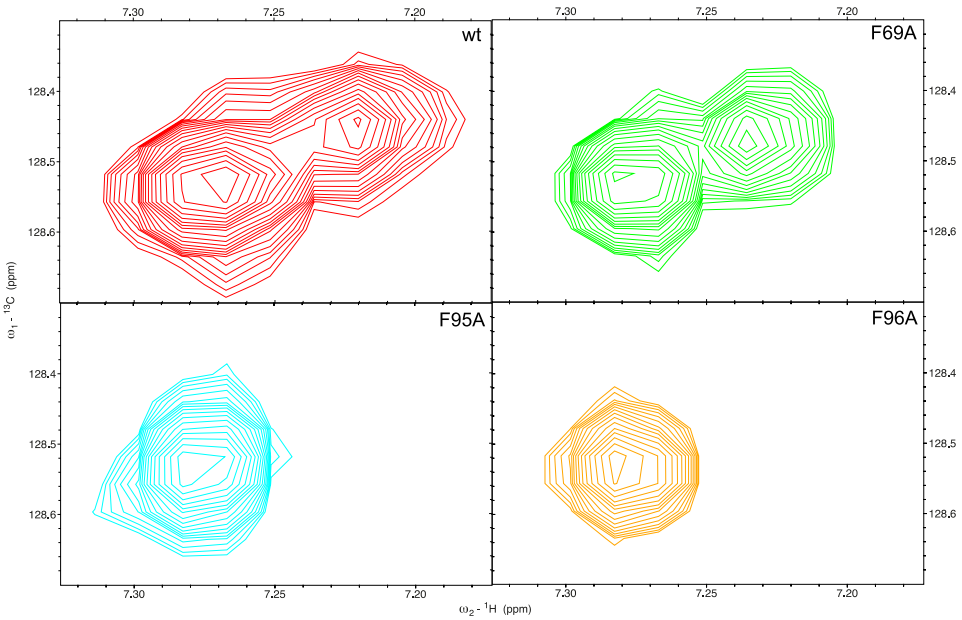

Fig. S1: 1H-13C HSQCs of labeled phenylalanine side-chains

YAP Mutations	Av IC_{50} (nM)	SD
D60C	12	2
A71C	9	2
V80C	4	1
K90C	12	1
S103C	2.9	0.4
A112C	3	1
T119C	5	1
S137C	5.3	0.4
S138C	4	1
S149C	2.6	0.4
Q158C	2.9	0.4
S164C	1.9	0.4
172C (insertion)	7	1
wt	11	1

Table S1: Potency of PRE mutants. The potency of the different mutant was measured in a TR-FRET assay ($n \geq 2$).

	Sequences of the oligonucleotides (5'-3')	
D60C	GATCGTGCACGTCCGCGGGTGCTCGGAGACCGACCTGGAGGCG	CGCCTCCAGGTCGGTCTCCGAGCACCCGCGGACGTGCACGATC
A71C	CCTGGAGGCGCTCTTCAACTGCGTCATGAACCCCAAGACGGC	GCCGTCTTGGGGTTCATGACGCAGTTGAAGAGCGCCTCCAGG
V80C	GAACCCCAAGACGGCCAACTGTCCCCAGACCGTGCCCATGAGGC	GCCTCATGGGCACGGTCTGGGGACAGTTGGCCGTCTTGGGGTTC
K90C	CCGTGCCCATGAGGCTCCGGTGTCTGCCCGACTCCTTCTTCAAGC	GCTTGAAGAAGGAGTCGGGCAGACACCGGAGCCTCATGGGCACGG
S103C	CCGCCGGAGCCCAAATGCCACTCCCGACAGGCCAG	CTGGCCTGTCGGGAGTGGCATTTGGGCTCCGGCGG
A112C	CCCGACAGGCCAGTACTGATTGTGGCACTGCAGGAGCCCTGAC	GTCAGGGCTCCTGCAGTGCCACAATCAGTACTGGCCTGTCGGG
T119C	GGCACTGCAGGAGCCCTGTGTCCACAGCATGTTCGAGCTC	GAGCTCGAACATGCTGTGGACACAGGGCTCCTGCAGTGCC
S127C	CCACAGCATGTTCGAGCTCATTGCTCTCCAGCTTCTCTGCAGTTG	CAACTGCAGAGAAGCTGGAGAGCAATGAGCTCGAACATGCTGTGG
S138C	GCAGTTGGGAGCTGTTTGTCCTGGGACACTGACCCCCACTGG	CCAGTGGGGGTCAGTGTCCCAGGACAAACAGCTCCCAACTGC
S149C	GTGGGTGTAGCTGCTGGGCCACAGACTACTCCAGTGGGGGTC	GACCCCCACTGGAGTAGTCTGTGGCCCAGCAGCTACACCCAC
Q158C	CCCAGCAGCTACACCCACAGCTTGTCATCTTCGACAGTCTTC	GAAGACTGTCGAAGATGACAAGCTGTGGGTGTAGCTGCTGGG
S164C	GCTCAGCATCTTCGACAGTCTTGTTTTGAGATACCTGATGATG	CATCATCAGGTATCTCAAAACAAGACTGTCGAAGATGCTGAGC
172C	GAGATACCTGATGATGTATGTTAACGCCATTAACCTGATGTTCTGG	CCAGAACATCAGGTTAATGGCGTTAACATACATCATCAGGTATCTC
L65A	CGGGGACTCGGAGACCGACGCGGAGGCGCTCTTCAACGCCG	CGGCGTTGAAGAGCGCCTCCGCGTCGGTCTCCGAGTCCCCG
L68A	GGAGACCGACCTGGAGGCGGCCTTCAACGCCGTCATGAACC	GGTTCATGACGGCGTTGAAGGCCGCCTCCAGGTCGGTCTCC
F69A	CCGACCTGGAGGCGCTCGCCAACGCCGTCATGAACCCC	GGGGTTCATGACGGCGTTGGCGAGCGCCTCCAGGTCGG
M86A	GTGCCCCAGACCGTGCCCGCGAGGCTCCGGAAGCTGCCC	GGGCAGCTTCCGGAGCCTCGCGGGCACGGTCTGGGGCAC
R89A	GACCGTGCCCATGAGGCTCGCGAAGCTGCCCGACTCCTTC	GAAGGAGTCGGGCAGCTTCGCGAGCCTCATGGGCACGGTC

L91A	GCCCATGAGGCTCCGGAAGGCCCCCGACTCCTTCTTCAAGC	GCTTGAAGAAGGAGTCGGGGGCCTTCCGGAGCCTCATGGGC
F95A	GGAAGCTGCCCGACTCCGCCTTCAAGCCGCCGGAGCCC	GGGCTCCGGCGGCTTGAAGGCGGAGTCGGGCAGCTTCC
F96A	GGAAGCTGCCCGACTCCTTCGCCAAGCCGCCGGAGCCCAAATCCC	GGGATTTGGGCTCCGGCGGCTTGGCGAAGGAGTCGGGCAGCTTCC

Table S2: Oligonucleotides used to produce the different YAP mutants via PCR-mediated mutagenesis. The first column denotes the introduced mutation with the two respective primers in the second and third column, Related to STAR Methods.

PART III

Concluding Discussion

The objective of this dissertation was to investigate the structural, dynamic, and functional properties of intrinsically disordered proteins (IDPs). We used NMR spectroscopy to elucidate the molecular mechanisms underlying YAP's interaction with TEAD and its regulatory roles. The concluding discussion synthesizes the main findings of the included publications, demonstrating how they collectively enhance our understanding of YAP's structure, conformational dynamics, and interaction with TEAD. It then explores the functional implications of these dynamics, particularly in the context of the Hippo signaling pathway and YAP:TEAD complex formation. A critical evaluation of the methodologies employed follows, assessing their strengths and limitations. This section also situates the research within the broader scientific literature, highlighting its unique contributions and points of convergence or divergence with previous studies. The discussion concludes by outlining potential directions for future research in this area.

10) Synthesis of Key Findings

The first publication constituted a foundational step in understanding the structural dynamics of YAP, offering detailed NMR resonance assignments for the fragment spanning residues 50–171[1]. This fragment encompasses the pivotal TEAD-binding domain, which plays a critical role in YAP's functionality within the Hippo pathway. The full backbone and partial side-chain assignments yielded a dataset essential for subsequent structural and dynamic analyses. Furthermore, the study described an efficient expression and purification protocol for the YAP fragment developed in the course of this dissertation. This protocol enabled the production of high yields of isotopically labeled YAP, thereby overcoming a possible limitation in NMR-based investigations of intrinsically disordered proteins (IDPs). It also addressed specific shortcomings of earlier protocols[2] that did not yield sufficient quantities of YAP when cultured in isotopically enriched M9 minimal medium[3].

The chemical shift data obtained from the assignment confirmed the presence of transient structural elements within the apo form of YAP. Despite its classification as an IDP, YAP displayed significant secondary structure propensity in regions corresponding to the β-strand and α-helix of the TEAD-binding interface. This finding challenged the conventional perception of IDPs as entirely unstructured and suggested a functional role for transient structure in mediating molecular recognition events. Such structural predisposition in IDPs has been increasingly recognized as a crucial element for modulating partner specificity and binding kinetics[4].

Building on this groundwork, the second publication focused on the conformational dynamics and interaction mechanisms of YAP[5]. Using a suite of NMR techniques combined with site-directed mutagenesis, the study demonstrated that apo YAP adopts several compact conformations that are stabilized through intramolecular interactions. The conformational landscape of YAP was shown to be defined by the interplay of its preformed β-strand, α-helix, and Ω-loop, whose interdependence

was further confirmed by perturbation through single-residue mutations. These mutations not only destabilized local secondary structures but also disrupted long-range contacts, leading to a global loss of compaction.

Selective side-chain labeling combined with NOE experiments identified long-range intramolecular contacts within the Ω-loop, notably between M86, L91, and F95/96, that are consistent with hydrophobic clustering. Mutational analysis involving key residues in the regions of the α-helix, and Ω-loop such as L65, L68, F69, M86, R89, L91, F95, and F96 resulted in a pronounced reduction of secondary structure propensity in both secondary structure elements in a co-dependent manner. These effects were further substantiated by paramagnetic relaxation enhancement (PRE) and diffusion-ordered spectroscopy (DOSY) measurements, which confirmed that apo YAP exists in a conformational equilibrium that includes a compact, preconfigured ensemble competent for TEAD binding that is even more compact than the bound state of YAP. This structural behavior supports a binding mechanism predominantly based on conformational selection rather than induced fit by positioning critical binding interfaces, namely the α-helix and Ω-loop, in close proximity to prime YAP:TEAD complex formation.

Together, these two studies provide a coherent and detailed view of the structural and dynamic properties of YAP in its apo state. From initial assignments to structural analysis and dynamic characterization of apo YAP's structural ensemble, they reveal that apo YAP is not a featureless ensemble but instead samples a structured, compact subpopulation with pre-aligned TEAD-binding elements. This structural preformation enhances binding efficiency and specificity and exemplifies how intrinsic disorder may be evolutionarily harnessed for signaling fidelity. The way how IDPs exhibit regulatory potential through transition between compact substates and extended disordered forms[6] is elegantly illustrated by the dynamic profile of YAP.

11) Implications of YAP's Structural Dynamics

The findings from this work underscore that structural priming and compaction in apo YAP are central to its functional role in the Hippo pathway. The pathway itself plays a pivotal role in regulating organ size, proliferation, and apoptosis through TEAD-mediated transcriptional activation[7–9]. The discovery that YAP adopts a compact, preorganized conformation even in the absence of TEAD suggests a reduced energetic cost for binding and a mechanism optimized for rapid response to upstream cues.

This preformed structural ensemble parallels mechanisms described in other IDPs, which frequently rely on residual structure and long-range intramolecular contacts to facilitate partner recognition[10–13]. The model of conformational selection posits that only those substates within the IDP conformational ensemble that are compatible with the binding partner become stabilized, offering both kinetic and thermodynamic advantages in complex formation.

Therapeutically, these insights open new avenues for targeting the YAP:TEAD interaction. The structural definition of apo YAP provides a rational framework for inhibitor design that disrupts the compact state or masks key binding elements. Verteporfin and hexasubstituted dipyrrins, for instance, are small molecules that have been shown to inhibit YAP function, potentially by binding to YAP and destabilizing the compact apo ensemble[14,15]. The ability to interfere with preformed binding elements before TEAD engagement suggests an alternative strategy to traditional orthosteric inhibition[16]. This approach mirrors similar advances in IDP-targeted drug development, where binding to the disordered free state has yielded promising results in modulating interactions in systems such as α-synuclein and tau[17,18]

Finally, the comparison of the observed YAP decompaction upon single-site mutations confirms that disruption of secondary structure elements or their

stabilizing interactions leads to altered association rates and decreased binding affinities[2]. These kinetic consequences further support the notion that structural preorganization in YAP is not incidental but central to its biological function.

In summary, apo YAP displays a dynamic yet structurally enriched ensemble primed for rapid and specific interaction with TEAD. This view reinforces the concept that functional disorder entails a continuum of structural states that can be selectively exploited for cellular regulation and offer potential targets for therapeutic intervention.

12) Methodological Considerations

The study of IDPs through NMR spectroscopy requires the integration of complementary techniques to elucidate the relationship between structure and dynamics, while remaining aware of the inherent limitations of each method. This is particularly evident in the case of the YAP, whose TEAD-binding domain adopts a dynamic ensemble of conformations in the apo state. Investigating this conformational heterogeneity at atomic resolution necessitated a combined approach utilizing the calculation of secondary structure propensities (SSP) from chemical shift data, PRE, DOSY, and specific isotope labeling of side-chains for NOE experiments.

Secondary structure propensity (SSP) scores determined by chemical shift data

One of the central techniques employed to characterize local secondary structure in YAP and identify the co-dependence of the different secondary structure elements was the calculation of SSP scores from chemical shift data. The SSP method relies on backbone ^{1}H, ^{15}N, $^{13}C\alpha$, and $^{13}C\beta$ chemical shifts and compares the observed shifts with random coil reference values to quantify the likelihood of a residue adopting α-helical or β-sheet conformations[19]. While this method is powerful for detecting secondary structure tendencies in IDPs, it assumes a linear correlation between chemical shift deviation and secondary structure content. This assumption

may break down in regions with complex or non-canonical structure, such as loops. Furthermore, the accuracy of SSP scores is highly sensitive to the quality of chemical shift assignments and reference data. This necessitated careful validation of the assignments of all different mutations. In addition, all our SSP results were interpreted in conjunction with complementary measurements such as ^{15}N transversal relaxation rates. These experiments then also allowed to detect the preformation in the Ω-loop region that is not detectable through SSP scores.

Specific side-chain labeling

To gain residue-specific insights into the preformation of the Ω-loop region through NOEs that may arise from the formation of a hydrophobic core by several hydrophobic residues in the Ω-loop region, selective side-chain isotope labeling was used. This involved metabolic incorporation of ^{13}C-labeled aromatic and aliphatic precursors ($^{13}C\varepsilon$-M, labeled phenylalanine and leucine ketoacids) in M9 minimal media, based on established protocols[20,21].

In IDPs, the use of NOE experiments to identify long-range contacts presents distinct challenges, primarily due to the fast internal motion and the usual lack of stable structures. As a result, many NOEs are averaged out or appear weak, making it difficult to distinguish genuine long-range contacts from spin diffusion or local contacts that transiently mimic long-range proximity[22,23]. This issue is further complicated by the high degree of signal overlap typical in IDPs, which makes spectral interpretation difficult. This was addressed by the described use of selective side-chain isotope labeling which drastically reduces spectral complexity and permits direct observation of side-chain NOEs. While this selective visibility enhances the detectability of otherwise obscured NOEs, it also introduces the risk of biased interpretation, as the observable NOEs are often restricted to more rigid or hydrophobically clustered regions and will be affected by the structural heterogeneity of the protein ensemble. Therefore, the use of side-chain NOEs in IDPs must be considered qualitative and does not allow to calculate inter-proton

distances. In YAP, the combination of M, F, and L side-chain labeling significantly enhanced spectral resolution in the $^{1}H–^{13}C$ HSQC spectra, effectively eliminating peak overlap for the targeted methyl and aromatic resonances. This improved resolution enabled the reliable assignment of side-chain signals, which in turn facilitated the identification of long-range NOEs observed in NOESY-based experiments between residues M86, L91, and F95/F96 in the Ω-loop, confirming the existence of a preformed hydrophobic core within this secondary structure element.

Paramagnetic relaxation enhancement (PRE)

To detect long-range transient contacts within the disordered YAP ensemble, PRE was employed through site-directed cysteine mutagenesis and subsequent spin labeling with (1-oxyl-2,2,5,5-tetramethyl-Δ3-pyrroline-3-methyl) methanethiosulfonate (MTSL). The MTSL tag introduces a paramagnetic center whose unpaired electron accelerates the transverse relaxation of nearby nuclei in an r^{-6}-dependent fashion. Thus, nuclei within ~25 Å of the label exhibit signal broadening, with nuclei in the so-called blind sphere (~6–10 Å) often completely quenched[24]. This approach has been widely used to successfully determine spatially encountering regions within IDPs[25–29].

PRE data were collected at multiple labeling positions along the whole YAP fragment placed about every tenth residue (D60C, A71C, V80C, K90C, etc.) summing up to a total of 12 different spin labeling positions. In addition to confirming the structural integrity of the PRE mutants via overlays of the ^{1}H-^{15}N HSQC spectra, we also measured their binding affinities to TEAD using TR-FRET competition assays to ensure that neither the global conformational ensemble nor complex formation was significantly altered by the introduction of mutation of the residues to a cysteine (see Supplemental Information of Feichtinger et al. 2022). Another important consideration in PRE measurements is the potential contribution of intermolecular effects as intermolecular PREs can mimic or obscure true intramolecular contacts, leading to erroneous conclusions about the conformational

ensemble or spatial proximity within the protein. In the case of YAP, these were ruled out through control experiments using 1:1 mixtures of ^{15}N-labeled YAP and ^{14}N MTSL-labeled YAP mutants. Specifically, PRE rates were measured for mixtures containing the spin-labeled mutants D60C, S103C, and S164C. In all cases, the evaluation revealed no significant PRE effects on the ^{15}N-labeled backbone of YAP, confirming that the observed relaxation enhancements arise from intramolecular interactions.

The experiments performed on YAP revealed extensive signal attenuation across residues 50–100, indicative of spatial proximity between the β-strand, α-helix, and Ω-loop regions in the apo state. While PRE is uniquely suited for capturing low-populated, transient structural states, its interpretation is constrained by the ensemble averaging of relaxation effects and its hypersensitivity to rare but close-contact states[30]. Nevertheless, as compaction and structural preformation has been reported as being closely tied to IDP functions, one can assume that these low-populated compact states that come up through the methodology are of significance and, therefore, of particular interest when investigating IDP functions. Furthermore, correlation matrices were constructed from PRE datasets to uncover structural coupling patterns, a method previously validated for other IDPs[31]. In the case of YAP, this analysis revealed a compact conformational subensemble in which the β-strand, α-helix, and Ω-loop regions exhibit coordinated long-range interactions, supporting the presence of a preorganized structural topology in the apo state.

Diffusion ordered spectroscopy (DOSY)

Complementary to PRE, we employed DOSY to assess the global compaction of YAP and its mutants. DOSY measures translational diffusion coefficients by applying pulsed-field gradients and tracking signal attenuation as a function of diffusion time[32–34]. The hydrodynamic radius inferred from the diffusion coefficient (D) via the Stokes–Einstein equation provides a coarse-grained proxy for molecular

compaction. In the case of IDPs, DOSY is used to detect the presence of secondary structure elements or hydrophobic clusters that will reduce the hydrodynamic radius of the conformational ensemble[35,36]. In line with previous studies applying DOSY to IDPs, it must be considered that IDPs are often sensitive to concentration-dependent effects, including aggregation and altered conformational equilibria, which may skew diffusion-based assessments of molecular size. Furthermore, the application of the Stokes–Einstein equation to calculate hydrodynamic radii assumes a globular, isotropic shape. Despite the established use of hydrodynamic radius as a proxy for more elongated conformational ensembles, as typically observed in IDPs, it is important to note that values derived from DOSY for such systems should be interpreted as apparent, ensemble-averaged quantities. Environmental parameters such as temperature and buffer viscosity must also be tightly controlled, as minor fluctuations can propagate into substantial deviations in D. Finally, the inclusion of internal standards such as dioxane can aid in calibrating gradient strength, but differences in buffer interaction profiles between standards and charged IDPs may introduce additional uncertainty[37].

We had to address these issues and the additional challenge that changes in a smaller compact part (residues 50-103) introduced by the mutation of a single residue (e.g. L68A) of the protein may not be properly distinguishable from the unaltered construct due to the more extended and flexible part (residues 104-171) of YAP having a bigger overall contribution to the hydrodynamic radius. To circumvent this, a new YAP construct ranging from residue 50 to 103 was produced. A comparison of the ^{1}H-^{15}N HSQC spectra exhibited a nearly perfect overlay of all peaks in the 50-103 construct and the same peaks in the full-length construct. The truncation, therefore, does not induce any significant changes in the structural ensembles. In addition, we closely monitored the addition of dioxane as our internal standard through ^{1}H-^{15}N HSQC. The spectra did not show any peak shifts that were introduced through the addition of the dioxane. The resulting spectra from the

DOSY measurements with the smaller construct also had much less signal overlap than the full construct and, therefore, allowed to derive diffusion coefficients for different mutations. Notably, mutants such as L68A and F95A exhibited decreased diffusion rates, consistent with an expanded conformational ensemble and increased hydrodynamic radius through the weakening of the hydrophobic clustering.

However, the observed changes in D are rather small as in comparison to PRE the observation reflects changes in the whole structural ensemble of YAP. Considering that only a smaller sub-population of YAP may be adopting that confirmational compact state and even modest conformational changes may fall below detection limits of DOSY experiments, it is nevertheless surprising to clearly detect differences that are in alignment with the findings from the PRE measurements. Despite all these limitations, the consistency of our DOSY-derived diffusion coefficients with PRE-based compaction trends supports the robustness of our experimental design and interpretation.

In summary, the investigation of YAP's structural dynamics in the apo state required a carefully orchestrated integration of complementary NMR techniques, each tailored to overcome specific limitations inherent to the study of intrinsically disordered proteins. SSP scores provided initial insights into secondary structure propensities, while their limitations in detecting non-canonical elements such as the Ω-loop were addressed through ^{15}N relaxation measurements and NOE-based detection of hydrophobic clustering. Selective side-chain labeling allowed for targeted probing of structurally informative NOEs despite the dynamic averaging and signal overlap typical of disordered systems. PRE measurements enabled the identification of long-range intramolecular contacts, with rigorous controls excluding intermolecular artifacts and ensuring that cysteine mutations did not perturb the native conformational ensemble. Finally, DOSY offered a complementary perspective on global compaction, with careful construct design

and experimental calibration ensuring interpretable data even in the context of minor population shifts. Taken together, these methodologies provided a multi-scale view of structural preformation in YAP and can serve as a framework for the systematic characterization of conformational ensembles in other functionally relevant IDPs with similar properties as YAP.

13) Related Works

This section discusses how the findings of the dissertation advance, complement, or challenge models on the molecular mechanism of the YAP:TEAD interaction as described in other studies.

Chen et al. (2010) and Li et al. (2010): Initial Structural Characterization of YAP:TEAD Complex

Both studies[38,39] independently reported the first high-resolution structures of the human YAP:TEAD complex, revealing that the TEAD-binding domain of YAP (residues 50 to 100) adopts a conserved fold, composed of a short β-strand, an α-helix with a central LxxLF motif, and a distinctive Ω-loop. These elements interact with complementary hydrophobic and electrostatic pockets on the surface of TEAD, which remains largely rigid and preorganized. Both studies interpreted YAP as an intrinsically disordered protein that folds only upon binding. The dissertation builds on this foundational model, but demonstrates that YAP's TEAD-binding domain is not fully disordered in its apo form. Our analysis reveals structural preformations in all three binding interfaces, supporting a binding mechanism with a substantial conformational selection component. Our findings refine the original structural paradigm by showing that YAP approaches TEAD not as a blank slate but as a partially pre-organized ensemble.

Mesrouze et al. (2017): Mutational Dissection of YAP:TEAD Interface

This study[2] performed alanine-scanning and double-mutant cycle analysis on both YAP and TEAD to quantify the contribution of interfacial residues and their coupling energies. The study provided a quantitative interaction map, solidifying that the Ω-loop acts as a binding hot spot whereas the N-terminal β-strand and the α-helix act more to orient and scaffold the loop and only have a moderate contribution to the binding. While this study provided the static energetic landscape of the interface, the dissertation adds the dynamic and kinetic dimensions. Thus, our results extend the findings of this study backward to the apo state as the network of interactions they mapped between YAP and TEAD (R89–E272^{TEAD4}, S94–Y429^{TEAD4}, F95 packing) is not only operative in the bound complex but already preformed in apo YAP.

Bokhovchuk et al. (2020): Model for Binding Mechanism as Helix-First Binding

This study[40] investigated the binding mechanism and kinetics of YAP:TEAD complex formation. Using stopped-flow kinetics and Φ-value analysis, the authors suggested that the association follows an apparent one-step mechanism involving internal structure formation during the transition state. A key insight was that YAP's α-helix folds and engages TEAD early, during or before the transition state, while the Ω-loop binds later in the process. Linear free energy (Φ) analysis supported this interpretation: mutations in the helix (L65A, F69A) yielded high Φ-values (~0.8–1.0), indicating these residues are structured in the transition state ensemble, whereas Ω-loop mutations produced much lower Φ-values (closer to 0), consistent with delayed folding and engagement. No stable intermediate was detected in the kinetic traces, implying that helix docking and loop closure are tightly coupled in time.

These findings align well with our data, which show that mutations in the LxxLF motif of the α-helix have the strongest impact on the overall compaction of apo YAP, suggesting that this segment plays a central role in influencing binding kinetics.

Helical preformation appears to serve as a scaffold that promotes the formation and co-stabilization of the β-strand and Ω-loop. The resulting compact substate facilitates rapid formation of an initial encounter complex, which then undergoes final adjustments to achieve the fully bound conformation. This step likely occurs on the nanosecond timescale and may have escaped detection by the employed kinetic methods in the study.

14) Future Research Perspectives

Building on the insights gained into apo YAP's preformed compact conformations in the TEAD-binding domain, a future research direction would be investigating the effect of S127 phosphorylation either through site-specific phosphorylation or the use of a phosphomimetic S127E variant. Our PRE correlation analysis revealed a structurally coupled region centered around S127 where the 14-3-3 binding is located. Changes in long-range PREs or global compaction upon phosphorylation would clarify how this modification allosterically remodels YAP's conformational ensemble. Furthermore, the dynamic behavior of YAP's binding interfaces within the fully assembled YAP:TEAD complex remain largely unexplored and combining PRE mapping on the complex with relaxation-dispersion experiments could reveal additional features that have not been explored yet.

To further build upon the work of tightly mapping PRE effects over the whole protein, paramagnetic relaxation interference (PRI) measurements could be performed. In PRI, a protein is labeled with two paramagnetic tags, and one measures how the combined effect on nuclear relaxation deviates from the sum of the individual PREs. These interference effects arise only when both spin labels transiently approach the same nucleus and allow to observe cooperative structural fluctuations and compact sub-states[29,31]. Additional insights could be gained by measuring ^{13}C-detected PREs placing paramagnetic tags near ^{13}C-labeled side chains to resolve side-chain proximity networks with improved resolution[41].

Combing this approach with selective ^{13}C labeling of key hydrophobic residues could allow to map the detailed architecture of the compaction of the TEAD-binding domain in apo and pre-encounter states.

As our work suggests that the compact substate of apo YAP precedes formation of the YAP:TEAD complex, this substate may represent a promising target for pharmacological inhibition of YAP:TEAD interaction. As a first step, compounds previously reported to bind YAP, such as Verteporfin[15] and hexasubstituted dipyrrins[14], could be evaluated for their effects on the structural ensemble of the apo state. In addition, a focused screen of small molecules could identify candidates that selectively destabilize the compact ensemble, shift YAP toward more extended conformations, and serve as leads for novel inhibitors that prevent TEAD engagement.

15) Concluding Remarks

This dissertation advances our understanding of IDPs by providing the first atomic-resolution characterization of the apo state of YAP's TEAD-binding domain. By integrating different NMR techniques with site-directed mutagenesis, the work revealed that YAP adopts a surprisingly compact conformational ensemble prior to TEAD engagement. This compaction, driven by long-range interactions between preformed secondary structure elements, particularly the α-helix and the Ω-loop, suggests a conformational selection mechanism rather than induced fit during complex formation. The discovery that these structural features are not only preformed but co-stabilized could be described best as dynamic compaction as a regulatory intermediate.

The key contribution of this work lies in demonstrating that YAP, though classified as an IDP, forms compact substates that are structurally and kinetically competent for partner binding. This challenges the prevailing view of IDPs as entirely disordered and functionally passive until interaction. These findings also open up

new avenues for (un)structure-based drug design by highlighting the compact apo state as a potential target for YAP:TEAD inhibition.

16) References

1. Feichtinger, M. *et al.* 1H, 13C, 15N resonance assignment of human YAP 50–171 fragment. *Biomol. NMR Assign.* **12**, 179–182 (2018).
2. Mesrouze, Y. *et al.* Dissection of the interaction between the intrinsically disordered YAP protein and the transcription factor TEAD. *eLife* **6**, e25068 (2017).
3. Marley, J., Lu, M. & Bracken, C. A method for efficient isotopic labeling of recombinant proteins. *J. Biomol. NMR* **20**, 71–75 (2001).
4. Wright, P. E. & Dyson, H. J. Intrinsically disordered proteins in cellular signalling and regulation. *Nat. Rev. Mol. Cell Biol.* **16**, 18–29 (2015).
5. Feichtinger, M. *et al.* Long-range structural preformation in yes-associated protein precedes encounter complex formation with TEAD. *iScience* **25**, 104099 (2022).
6. Fuxreiter, M. Classifying the Binding Modes of Disordered Proteins. *Int. J. Mol. Sci.* **21**, 8615 (2020).
7. Yu, F.-X., Zhao, B. & Guan, K.-L. Hippo Pathway in Organ Size Control, Tissue Homeostasis, and Cancer. *Cell* **163**, 811–828 (2015).
8. Fu, M. *et al.* The Hippo signalling pathway and its implications in human health and diseases. *Signal Transduct. Target. Ther.* **7**, 376 (2022).
9. Ma, S., Meng, Z., Chen, R. & Guan, K.-L. The Hippo Pathway: Biology and Pathophysiology. *Annu. Rev. Biochem.* **88**, 577–604 (2019).

10. Mittag, T. *et al.* Structure/Function Implications in a Dynamic Complex of the Intrinsically Disordered Sic1 with the Cdc4 Subunit of an SCF Ubiquitin Ligase. *Structure* **18**, 494–506 (2010).
11. Arai, M., Sugase, K., Dyson, H. J. & Wright, P. E. Conformational propensities of intrinsically disordered proteins influence the mechanism of binding and folding. *Proc. Natl. Acad. Sci.* **112**, 9614–9619 (2015).
12. Newcombe, E. A., Delaforge, E., Hartmann-Petersen, R., Skriver, K. & Kragelund, B. B. How phosphorylation impacts intrinsically disordered proteins and their function. *Essays Biochem.* **66**, 901–913 (2022).
13. Elkjær, S. *et al.* Evolutionary fine-tuning of residual helix structure in disordered proteins manifests in complex structure and lifetime. *Commun. Biol.* **6**, 63 (2023).
14. Gibault, F. *et al.* Molecular Features of the YAP Inhibitor Verteporfin: Synthesis of Hexasubstituted Dipyrrins as Potential Inhibitors of YAP/TAZ, the Downstream Effectors of the Hippo Pathway. *ChemMedChem* **12**, 954–961 (2017).
15. Liu-Chittenden, Y. *et al.* Genetic and pharmacological disruption of the TEAD–YAP complex suppresses the oncogenic activity of YAP. *Genes Dev.* **26**, 1300–1305 (2012).
16. Crawford, J. J., Bronner, S. M. & Zbieg, J. R. Hippo pathway inhibition by blocking the YAP/TAZ–TEAD interface: a patent review. *Expert Opin. Ther. Pat.* **28**, 867–873 (2018).
17. Kiss, R. *et al.* Structural Basis of Small Molecule Targetability of Monomeric Tau Protein. *ACS Chem. Neurosci.* **9**, 2997–3006 (2018).

18. Tóth, G. *et al.* Novel Small Molecules Targeting the Intrinsically Disordered Structural Ensemble of α-Synuclein Protect Against Diverse α-Synuclein Mediated Dysfunctions. *Sci. Rep.* **9**, 16947 (2019).

19. Marsh, J. A., Singh, V. K., Jia, Z. & Forman-Kay, J. D. Sensitivity of secondary structure propensities to sequence differences between α- and γ-synuclein: Implications for fibrillation. *Protein Sci.* **15**, 2795–2804 (2006).

20. Lichtenecker, R. J., Weinhäupl, K., Schmid, W. & Konrat, R. α-Ketoacids as precursors for phenylalanine and tyrosine labelling in cell-based protein overexpression. *J. Biomol. NMR* **57**, 327–331 (2013).

21. Schörghuber, J. *et al.* Late metabolic precursors for selective aromatic residue labeling. *J. Biomol. NMR* **71**, 129–140 (2018).

22. Dyson, H. J. & Wright, P. E. Unfolded Proteins and Protein Folding Studied by NMR. *Chem. Rev.* **104**, 3607–3622 (2004).

23. Mittag, T. & Forman-Kay, J. D. Atomic-level characterization of disordered protein ensembles. *Curr. Opin. Struct. Biol.* **17**, 3–14 (2007).

24. Bertini, I., Luchinat, C., Parigi, G. & Ravera, E. *NMR of Paramagnetic Molecules: Applications to Metallobiomolecules and Models*. (Elsevier, Amsterdam, Netherlands, 2017).

25. Konrat, R. NMR contributions to structural dynamics studies of intrinsically disordered proteins. *J. Magn. Reson.* **241**, 74–85 (2014).

26. Salmon, L. *et al.* NMR Characterization of Long-Range Order in Intrinsically Disordered Proteins. *J. Am. Chem. Soc.* **132**, 8407–8418 (2010).

27. Kristjansdottir, S. *et al.* Formation of Native and Non-native Interactions in Ensembles of Denatured ACBP Molecules from Paramagnetic Relaxation Enhancement Studies. *J. Mol. Biol.* **347**, 1053–1062 (2005).

28. Silvestre-Ryan, J., Bertoncini, C. W., Fenwick, R. B., Esteban-Martin, S. & Salvatella, X. Average Conformations Determined from PRE Data Provide High-Resolution Maps of Transient Tertiary Interactions in Disordered Proteins. *Biophys. J.* **104**, 1740–1751 (2013).

29. Kurzbach, D. *et al.* Detection of correlated conformational fluctuations in intrinsically disordered proteins through paramagnetic relaxation interference. *Phys. Chem. Chem. Phys.* **18**, 5753–5758 (2016).

30. Ganguly, D. & Chen, J. Structural Interpretation of Paramagnetic Relaxation Enhancement-Derived Distances for Disordered Protein States. *J. Mol. Biol.* **390**, 467–477 (2009).

31. Kurzbach, D. *et al.* NMR probing and visualization of correlated structural fluctuations in intrinsically disordered proteins. *Phys. Chem. Chem. Phys.* **19**, 10651–10656 (2017).

32. Pagès, G., Gilard, V., Martino, R. & Malet-Martino, M. Pulsed-field gradient nuclear magnetic resonance measurements (PFG NMR) for diffusion ordered spectroscopy (DOSY) mapping. *The Analyst* **142**, 3771–3796 (2017).

33. Groves, P. Diffusion ordered spectroscopy (DOSY) as applied to polymers. *Polym. Chem.* **8**, 6700–6708 (2017).

34. Johnson, C. S. Diffusion ordered nuclear magnetic resonance spectroscopy: principles and applications. *Prog. Nucl. Magn. Reson. Spectrosc.* **34**, 203–256 (1999).

35. Kosol, S., Contreras-Martos, S., Cedeño, C. & Tompa, P. Structural Characterization of Intrinsically Disordered Proteins by NMR Spectroscopy. *Molecules* **18**, 10802–10828 (2013).

36. Wilkins, D. K. *et al.* Hydrodynamic Radii of Native and Denatured Proteins Measured by Pulse Field Gradient NMR Techniques. *Biochemistry* **38**, 16424–16431 (1999).

37. Whitehead, R. D., Teschke, C. M. & Alexandrescu, A. T. Pulse-field gradient nuclear magnetic resonance of protein translational diffusion from native to NON-NATIVE states. *Protein Sci.* **31**, e4321 (2022).

38. Chen, L. *et al.* Structural basis of YAP recognition by TEAD4 in the Hippo pathway. *Genes Dev.* **24**, 290–300 (2010).

39. Tian, W., Yu, J., Tomchick, D. R., Pan, D. & Luo, X. Structural and functional analysis of the YAP-binding domain of human TEAD2. *Proc. Natl. Acad. Sci.* **107**, 7293–7298 (2010).

40. Bokhovchuk, F. *et al.* An Early Association between the α-Helix of the TEAD Binding Domain of YAP and TEAD Drives the Formation of the YAP:TEAD Complex. *Biochemistry* **59**, 1804–1812 (2020).

41. Mateos, B., Konrat, R., Pierattelli, R. & Felli, I. C. NMR Characterization of Long-Range Contacts in Intrinsically Disordered Proteins from Paramagnetic

Relaxation Enhancement in ^{13}C Direct-Detection Experiments. *ChemBioChem* **20**, 335–339 (2019).